

École doctorale n° 364 : Sciences Fondamentales et Appliquées

Doctorat ParisTech

THÈSE

pour obtenir le grade de docteur délivré par

L'École Nationale Supérieure des Mines de Paris

Spécialité doctorale “Science et Génie des Matériaux”

présentée et soutenue publiquement par

Ali SAAD

le xx mai 2015

NUMERICAL MODELLING OF MACROSEGREGATION INDUCED BY SOLIDIFICATION SHRINKAGE IN A LEVEL SET APPROACH

Directeurs de thèse: **Michel BELLET**
Charles-André GANDIN

Jury

M. Blablabla ,	Professeur, MINES ParisTech	Rapporteur
M. Blablabla ,	Professeur, Arts Et Métiers ParisTech	Rapporteur
M. Blablabla ,	Chargé de recherche, ENS Cachan	Examinateur
M. Blablabla ,	Danseuse, en freelance	Examinateur
M. Blablabla ,	Ingénieur, MIT	Examinateur

T
H
E
S
S

Contents

1 General Introduction	1
1.1 Solidification notions	2
1.1.1 Solute partitioning	2
1.1.2 Dendritic growth	4
1.1.3 Mush permeability	6
1.2 Macrosegregation	7
1.2.1 Liquid thermosolutal convection	7
1.2.2 Solidification shrinkage	8
1.2.3 Movement of equiaxed grains	8
1.2.4 Solid deformation	8
1.3 Other defects	8
1.4 Industrial Worries	10
1.5 Project context and objectives	11
1.5.1 Context	11
1.5.2 Objectives and outline	12
2 Modelling Review	15
2.1 Modelling macrosegregation	16
2.1.1 Macroscopic solidification model: monodomain	17
2.2 Eulerian and Lagrangian motion description	23
2.2.1 Overview	23
2.2.2 Interface capturing	25
2.3 Solidification models with level set	25
2.4 The level set method	26
2.4.1 Diffuse interface	27
2.4.2 Mixing Laws	28
2.5 Interface motion	30
2.5.1 Level set transport	31
2.5.2 Level set regularisation	32

Contents

3 Energy balance with thermodynamic tabulations	37
3.1 State of the art	38
3.2 Thermodynamic considerations	38
3.2.1 Volume averaging	38
3.2.2 The temperature-enthalpy relationship	39
3.2.3 Tabulation of properties	40
3.3 Numerical method	41
3.3.1 Enthalpy-based approach	45
3.3.2 Temperature-based approach	45
3.3.3 Convergence	46
3.4 Validation	47
3.4.1 Pure diffusion	47
3.4.2 Convection and diffusion	50
3.5 Application: multicomponent alloy solidification	53
3.5.1 Tabulations	55
3.5.2 Discussion	56
4 Macrosegregation with liquid metal motion	61
4.1 Introduction	62
4.2 Numerical treatment	62
4.2.1 Stable mixed finite elements	62
4.2.2 Variational multiscale (VMS)	62
4.3 VMS solver	63
4.4 Computational stability	64
4.4.1 CFL condition	64
4.4.2 Integration order	64
4.5 Application to multicomponent alloys	64
4.5.1 Results	66
4.6 Macroscopic freckle prediction	67
4.6.1 Introduction	69
4.6.2 Experimental work	70
4.6.3 Macroscopic scale simulations	70
4.7 Meso-Macro freckle prediction	77
4.7.1 Numerical method	77
4.7.2 Configuration	79
4.7.3 Effect of vertical temperature gradient	82
4.7.4 Effect of cooling rate	84
4.7.5 Effect of lateral temperature gradient	86
4.7.6 Mono-grain freckles	88

5 Macrosegregation with solidification shrinkage	89
5.1 Solidification shrinkage	90
5.2 Multidomain formalism	90
5.2.1 Assumptions	92
5.2.2 Mass balance	93
5.3 FE model: Metal	93
5.3.1 Mass and momentum conservation	93
5.3.2 Energy conservation	95
5.3.3 Species conservation	97
5.4 FE model: Air	99
5.4.1 Mass and momentum conservation	100
5.4.2 Energy conservation	100
5.4.3 Species conservation	100
5.5 FE monolithic model	100
5.5.1 Permeability mixing	100
5.5.2 Model equations	101
5.5.3 Interface treatment	101
5.6 Shrinkage without macrosegregation	103
5.6.1 Al-7wt% Si	104
5.6.2 Pb-3wt% Sn	104
5.7 Shrinkage with macrosegregation	104
5.7.1 Al-7wt% Si	104
5.7.2 Pb-3wt% Sn	104
Bibliography	105

Contents

Acronym	Standing for
ALE	Arbitrary Lagrangian-Eulerian
BTR	Brittleness temperature range
CCEMLCC	Chill Cooling for the Electro-Magnetic Levitator in relation with Continuous Casting of steel
CEMEF	Center for Material Forming
CSF	Continuum Surface Force
DLR	Deutsches Zentrum für Luft- und Raumfahrt
EML	Electromagnetic levitation
ESA	European Space Agency
FEM	Finite Element Method
GMAW	Gas Metal Arc Welding
ISS	International Space Station
IWT	Institut für Werkstofftechnik
LHS	Left Hand Side
LSM	Level set method
MAC	Marker-and-cell
MIN	Mini-element
PF	Phase field
RHS	Right Hand Side
RUB	Ruhr Universität Bochum
RVE	Representative Elementary Volume
SCPG	Shock Capturing Petrov-Galerkin
SUPG	Streamline Upwind Petrov-Galerkin
VMS	Variational MultiScale
VOF	Volume Of Fluid

Contents

Chapter 1

General Introduction

Casting is one the earliest production techniques created by human civilisation since the Bronze Age, dated to circa 3000 BC. From ancient swords to nowadays toys, the need for alloys has never decreased. The key phenomenon behind this technique is solidification, or the transformation of matter from liquid to solid state. With this phase change, many phenomena, not visible to the naked eye, take place with a very complex interaction, in order to form a solid. However, the combination of thermal phenomena, like release of latent heat of solidification, and chemical phenomena like redistribution of chemical element atoms (also known as solute) with other atoms, often lead to *segregation*. The origins of this word from Latin, *segregatus*, has a social meaning of "separating a group from the dominant majority", while in metallurgy it means a non uniform distribution of chemical species. Depending on the scale, we may speak of *microsegregation* when the heterogeneity spans some few hundred microns, whereas the term *macrosegregation* refers to a much coarser length scale, ranging from some millimetres to some meters ! The final solid structure is has intrinsic thermophysical and thermomechanical properties directly influenced by the segregation pattern. In casting processes, such as continuous casting ([fig. 1.7](#)) and ingot casting, it is crucial to apprehend these intricate phenomena leading to macrosegregation as well as the influence on the final product, at each step of the process.

In this introductory chapter, we give a quick overview of solidification phenomena and microstructure, then present the factors which promote segregation, on both microscopic and macroscopic scales. Aside from macrosegregation, others defects are also briefly presented.

In a continuous casting process ([fig. 1.1a](#)), the partially solidified slab is carried through a series of rolls that exert contact forces to straighten it. As the mushy part of a slab enters through these rolls, interdendritic liquid is expelled backwards, i.e. in regions with lower solid fraction. Since the slab edges solidify earlier than the centre, the enriched liquid accumulates halfway in thickness, forming a centreline macrosegregation as shown in [fig. 1.2](#). Other types of segregates (channels, A-segregates ...) can also be

Chapter 1. General Introduction

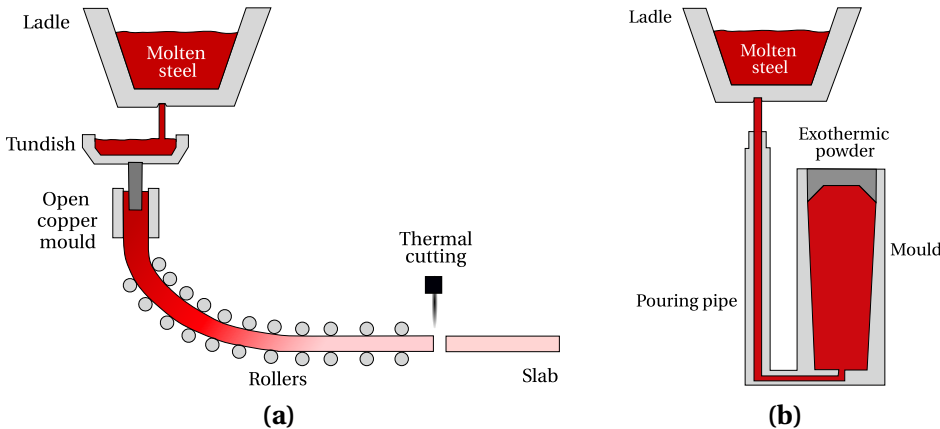


Fig. 1.1 – Main processes for steelmaking by (a) continuous casting or (b) ingot casting

found but remain more specific to ingot casting. A variety of segregation patterns can be encountered while casting heavy ingots, as in [fig. 1.1b](#):

- the lower part is characterized by a negative segregation cone promoted by the sedimentation of equiaxed crystals and settling of dendrite fragments,
- positive segregation channels, known as A-segregates, form along the columnar dendritic zones, close to the vertical contact with the mould,
- positive V-segregates can be identified in the centre of the ingot,
- a positive "hot-top" macrosegregation in the upper zone where the last rich liquid solidifies, caused by solidification shrinkage and thermosolutal buoyancy forces.

[Combeau et al. \[2009\]](#) state that A-segregates and V-segregates formation is mainly attributed to local flow phenomena. As such, their scale is finer than macrosegregation, hence called "mesosegregates".

1.1 Solidification notions

1.1.1 Solute partitioning

The simplest definition is of this phenomenon is an uneven distribution of solute between the liquid and the growing solid, at the microscopic scale of the interface separating these phases. If we consider a binary alloy, then the solubility limit is the key factor that dictates the composition at which a primary solid phase exists at equilibrium. The segregation (or partition) coefficient k determines the extent of solute rejection into the liquid during solidification:

$$k = \frac{w^{s^*}}{w^{l^*}} \quad (1.1)$$

1.1. Solidification notions

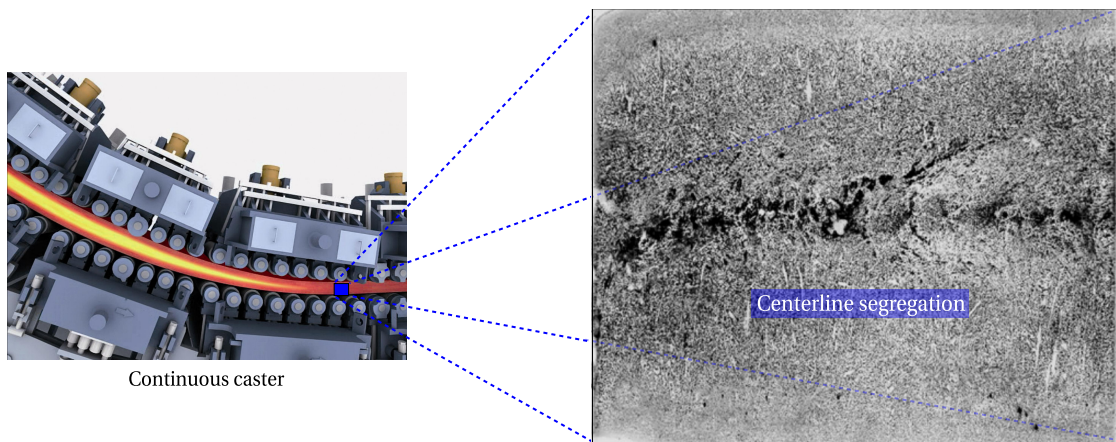


Fig. 1.2 – Zoom on a sulphur print of a continuously cast high carbon steel billet at a longitudinal section, showing high positive centreline segregation [Choudhary et al. 2007].

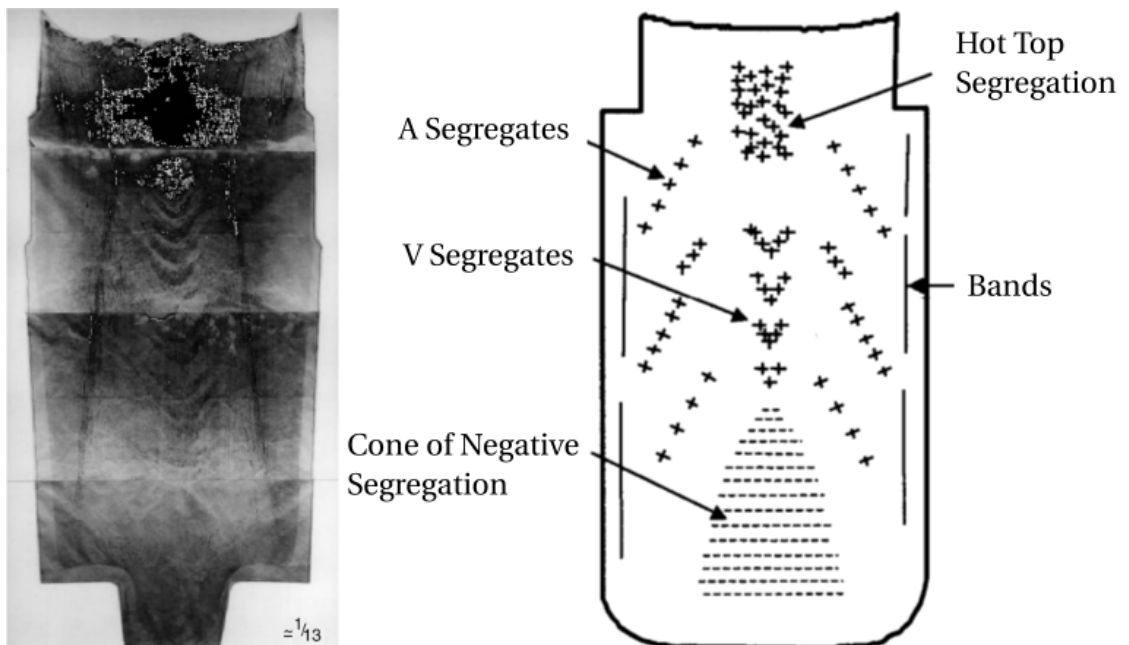


Fig. 1.3 – Sulphur print (left) of a 65-ton steel ingot [Lesoult 2005] showing various patterns (right) of macrosegregation [Flemings 1974]

Chapter 1. General Introduction

where w^{s*} and w^{l*} are the compositions of the solid and liquid respectively, at the interface. When the segregation coefficient is less than unity (such is the case for most alloys during dendritic solidification), the first solid forms at the liquidus temperature, T , with a composition $w^{s*} = kw^{l*} = kw_0$ less than the liquid's composition w_0 , the latter being initially at the nominal composition, w_0 . [Figure 1.4](#) illustrates a typical binary phase diagram where the real solidus and liquidus are represented by solid lines, while the possible linear approximations are in grey dashed lines. For most binary alloys, this linearisation simplifies derivation of microsegregation models, as k becomes independent of temperature.

For each phase, the relationship between the composition at the interface and that in the bulk depends on the chemical homogenisation (i.e. solute diffusivity) of the phase. The more homogeneous a phase, the closer the concentrations between the interface and the bulk, hence closer to equilibrium. It is thus essential to study the effect of homogenisation on the segregation behaviour and the subsequent effect on solidification, which is seen by a non-uniform composition through the cast product on a microscopic scale, better known as microsegregation. This phenomenon is essential in a casting process inasmuch as it affects the microstructure and grain morphology, hence the final mechanical properties of the alloy.

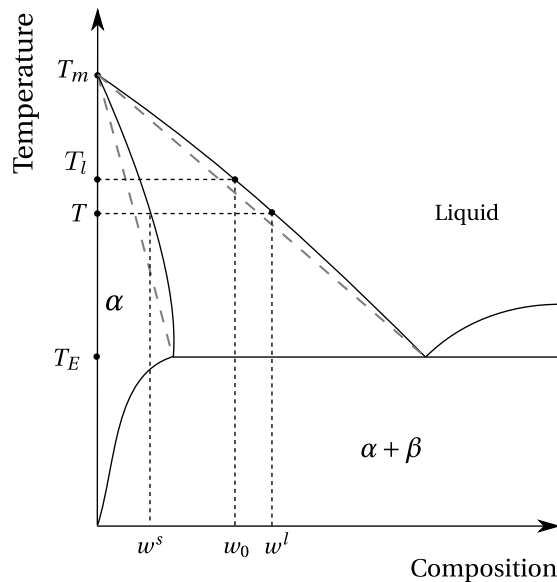


Fig. 1.4 – Typical eutectic phase diagram of a binary alloy showing the real solidus and liquidus at full equilibrium, with the corresponding linear approximations (grey dashed lines). T_m and T_E are respectively the melting point of the solvent and the eutectic temperature.

1.1.2 Dendritic growth

In a casting process, the chill surface i.e. the contact between the molten alloy and relatively cold moulds, is the first area to solidify. Thermal gradient, G , and cooling rate,

R , are two crucial process parameters that define the solid-liquid interface velocity, \vec{v}^* , which in turn affects the initial microstructure. Although it may be not easy to control them, their crucial role in solidification is well established.

The solid-liquid interface fluctuates when solidifying, thus perturbations may appear on the front, locally destabilizing it. Two outcome scenarios are possible. The



Fig. 1.5 – Time evolution of a solidifying Al-4 wt.% Cu sample, showing interface destabilisation and subsequent dendritic solidification [buffet_analysis_2011]. The liquid far from the interface and having a blue color is at nominal composition, while the one near the dendritic structure with the yellow and red colors, is richer in solute.

first scenario is characterized by low values of \vec{v}^* where the interface maintains a planar shape, hence we speak of *planar growth*. With this kind of growth, a random protuberance appearing at the interface, has a low tip velocity (low driving force of solidification). As such, the rest of the interface catches up, maintaining the planar geometry. In another scenario more representative of a real casting, the interface speed is greater in general, due to high solidification rate. The protuberance tip will be pulled into a liquid less rich in solute than the interface, as shown in the time frames of fig. 1.5. The zone ahead of the solid-liquid interface is constitutionally undercooled [Tiller et al. 1953], giving a greater driving force for the protuberance to grow in the direction of the thermal gradient. As the solid-liquid interface adopts a tree-like shape, we speak of *dendritic growth*. Near the chill surface, dendrites are columnar, with a favourable growth in the $<100>$ direction for alloys with cubic lattices, but different orientations are also reported in the literature [see Dantzig et al. 2009, p. 289]. Far from mould walls, a similar dendritic growth phenomenon occurs where temperature is uniform, but with an equiaxed morphology. Figure 1.6 shows both columnar and equiaxed morphologies. Columnar dendrites are characterised by a primary spacing, λ_1 , between the main trunks, and a secondary spacing, λ_2 , for the arms that are perpendicular to the trunks. It should be noted that λ_1 and λ_2 , together with the grain size, are three important microstructural parameters in the as-cast microstructure [Easton et al. 2011]. Further branching may occur but will not be discussed here.

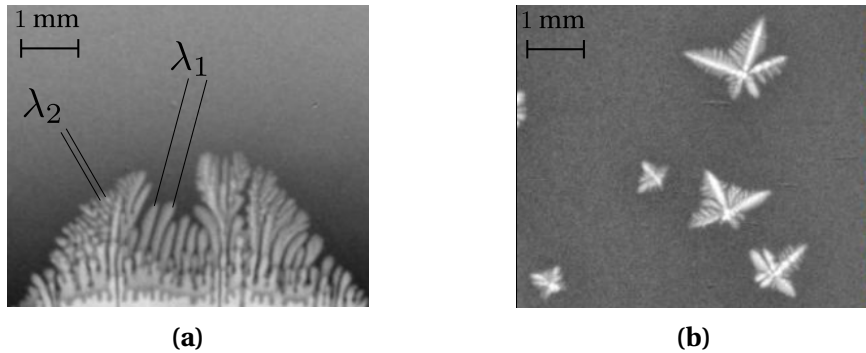


Fig. 1.6 – In situ observation by X-ray radiography of the (a) columnar microstructure for Al-4 wt.% Cu alloy [Buffet et al. 2010] and (b) equiaxed microstructure during solidification of Al-10 wt.% Cu alloy [Bogno et al. 2013].

1.1.3 Mush permeability

The dendritic geometry is crucial in solidification theory as it exhibits lower solid fraction compared to a microstructure formed by planar growth. This fact has consequences on the fluid-structure interaction in the mushy zone, namely the liquid flow through dendrites. At the chill surface, the solid grows gradually from dispersed growing nuclei to a permeable solid skeleton, until finally grains have fully grown at the end of phase change. In the intermediate state, the liquid flow in and out of the mushy zone through the dendrites is a key phenomenon from a rheological perspective. The flow through the solid skeleton is damped by primary and secondary dendrites, resulting in momentum dissipation just like in saturated porous media. The famous Darcy [1856] law relates the pressure gradient ($\vec{\nabla}p$) to the fluid velocity \vec{v} (assuming a the solid phase is fixed), through the following equation [Rappaz et al. 2003]:

$$\vec{v} = \frac{\mathbb{K}}{\mu^l} \vec{\nabla}p \quad (1.2)$$

where μ^l is the liquid dynamic viscosity and \mathbb{K} is the permeability tensor. The latter parameter has been the subject of numerous studies that aimed to predict it from various microstructural or morphological parameters. Some of these studies have started even before the first attempts to model macrosegregation by Flemings et al. [1967], Flemings et al. [1968a], and Flemings et al. [1968b]. Basically, all models include the solid fraction, g^s , as input to predict mush permeability along with empirical data. An instance of such models is the work of Xu et al. [1991]. Some models rely additionally on the primary dendrite arm spacing λ_1 like Blake-Kozeny [Ramirez et al. 2003], or the secondary dendrite arm spacing λ_2 like Carman-Kozeny, as a meaningful parameter to determine an isotropic permeability. Other models like Poirier [1987] and Felicelli et al. [1991] derive an anisotropic permeability based on both λ_1 and λ_2 .

The present work uses Carman-Kozeny as a constitutive model for the isotropic per-

meability scalar (zero order tensor):

$$\mathbb{K} = \frac{\lambda_2^2 g^{l^3}}{180 (1 - g^l)^2} \quad (1.3)$$

1.2 Macrosegregation

Macrosegregation generally stems from a solubility difference between a liquid phase and one or more solid phases, along with a relative velocity between these phases. While the former is responsible for local solute enrichment or depletion, the latter will propagate the composition heterogeneity on a scale much larger than just a few dendrites. This is why macrosegregation could be observed on the scale of a casting, up to several meters in length. While microsegregation can be healed by heat treatments, the alloy to speed up the diffusion process and allow homogenization, heterogeneities spanning on larger distances cannot be treated after solidification. It is obvious that macrosegregation is an irreversible defect. Failure to prevent it, may lead to a substantial decline in the alloy's mechanical behaviour and its serviceability. Experimental investigations of macrosegregation in steels were the subject of numerous studies in the past, like the work of [Lesoult \[2005\]](#) [for other references check 1996BeckermannSchneider](#). They were mainly motivated by industrial research that aimed at reducing defective production caused by macrosegregation. However, steel was not the only alloy that was investigated, probably because of its high melting point. Instead, many studies in the past relied on other metallic alloys as a replacement recourse, for their low melting points, also for their well-known thermophysical and mechanical properties, such as aluminium-based alloys (aluminium-copper or aluminium-silicon) [[Lesoult et al. 2001](#); [Ferreira et al. 2004](#); [Ferreira et al. 2009](#)] and lead-tin/tin-lead alloys[[Hebditch et al. 1974](#); [Prescott et al. 1994](#); [Hachani et al. 2012](#)]. Investigating macrosegregation was not only limited to metallic alloys, but also to organic compounds like the well-known sodium chloride [[Wanqi et al. 1989](#)]. Four main factors can (simultaneously) cause fluid flow leading to macrosegregation:

1.2.1 Liquid thermosolutal convection

During solidification, the liquid density undergoes changes due to temperature gradients. Generally for steels, an increasing temperature results in a lighter liquid phase and vice-versa. These variations create a driving force of thermal convection in the melt, during which chemical species are redistributed by convective transport. While a uniform composition is usually maintained throughout the liquid phase, solute gradients may appear in zones where thermal convection currents are not sufficient to homogenise the liquid solution. Similarly to thermal gradient, a solute gradient is behind liquid density variations. Nevertheless, the relationship between the liquid's

Chapter 1. General Introduction

composition and its density is a characteristic of the alloy. While for some alloys, a positive solute gradient creates a positive density gradient, for others the opposite is true, due to a heavier solute. Whether convection is solute or temperature dominated, convection currents are important in the formation of macrosegregation, especially that phase densities vary considerably upon cooling the superheated alloy to room temperature.

1.2.2 Solidification shrinkage

Solid alloys generally have a greater density than the liquid phase ($\rho^s > \rho^l$), thus occupy less volume, with the exception of silicon where the opposite is true. Upon solidification, the liquid moves towards the solidification front to compensate for the volume difference caused by the phase change, as well as the thermal contraction. When macrosegregation is triggered by solidification shrinkage, we speak of *inverse segregation*: while one would naturally expect negative macrosegregation near the contact with the chill, shrinkage-induced flow promotes the opposite phenomenon, by bringing solute-richer liquid towards the solidifying areas, thus raising their solute content, and resulting in a positively segregated solid. In contrast to liquid convection, shrinkage flow may cause macrosegregation even without gravity.

1.2.3 Movement of equiaxed grains

Globular and equiaxed dendritic grains nucleate and grow in the liquid bulk where thermal gradients are weak, or in the presence of inoculants. Consequently, they are transported by the flow, thus floating or sedimenting depending on their density [Beckermann 2002]. During their movement, the nearby liquid is driven away before the grains finally settle in the end of solidification. Since solute-rich liquid is expelled, a negative macrosegregation zone (often referred to as *negative segregation cone* in cast ingots) is detected in their final position.

1.2.4 Solid deformation

Stresses of thermal and mechanical nature are always found in casting processes (e.g. bulging between rolls in continuous casting). Deformation of the semi-solid in the mushy zone causes a relative solid-liquid flow in the inward (tensile stresses) or outward (compressive stresses) direction, causing macrosegregation.

1.3 Other defects

Defects are encountered in any industrial process. More importantly, a lot of them in the casting industry can be disastrous when the cast product is unserviceable and

rejected. This leads to a systematic product recycling, i.e. the product is ditched to be reheated (if possible), remelted and then cast again. From an economic point view, the operation is very expensive. Understanding and preventing defects when possible is thus crucial in the casting industry. We briefly list hereafter the main encountered defects.

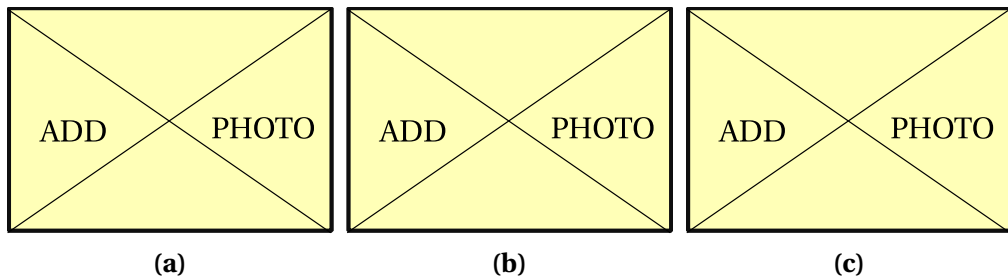


Fig. 1.7 – Three instances of solidification-related defects found in cast products: (a) asdads
(b) dfdsdf and (c) fdsfsf.

Hot tearing

This defect, also denoted solidification cracking or hot cracking, occurs in the mushy zone at high solid fractions when a failure or crack appears at specific locations, the hot spots. The temperature range in which the steel is vulnerable to hot tearing is known as the brittleness temperature range (BTR). It corresponds to solid fractions greater than 90%, where the liquid phase starts to form a discontinuous film. Many factors can initiate the failure, but the main origin is a lack of liquid feeding required to compensate for the solidification shrinkage, in the presence of thermal stresses in the mushy region. Therefore, a crack initiates and then propagates in the casting.

Porosity

Porosity is a void defect formed inside the casting or at the outer surface. It may be attributed to two different factors. Firstly, we speak of *shrinkage porosity*, when a void forms as a result of density differences between the liquid and its surrounding dendritic solid network, the latter being generally denser than the former. The second factor is the presence of dissolved gaseous phases in the melt. According to Dantzig et al. [2009], these gases may be initially in the melt, or created by the reaction between the metal and water found in the air or trapped in grooves at the moulds surface. Providing sufficient cooling and pressure drop in the liquid, the latter becomes supersaturated. The nucleation of a gaseous phase is then triggered.

Freckles or segregated channels

The origin of this defect is a combined effect of microsegregation and buoyancy forces. Upon solidification, solid forms while exchanging solutes with the liquid due to partitioning. For a solute species that preferentially segregates into the liquid (partition coefficient less than unity) and locally reduce the liquid density, a solutal driving force is created inside the mushy zone, generating convection currents, with "plume" shapes as often reported in the literature [Sarazin et al. 1992; Schneider et al. 1997; Shevchenko et al. 2013]. Temperature gradient is often an additional force of convection as the liquid density depends also temperature-dependent, the resulting driving force is then qualified as "thermosolutal".

1.4 Industrial Worries

Steel production has continuously increased over the years to meet the industrial needs. Figure 1.8 shows this increase between 1980 and 2013 with a clear dominance of the Chinese production. Quality constraints have also increased where specific grades of steel are needed in critical applications such as mega-structures in construction and heavy machinery. Therefore, alloys with defects are considered vulnerable and should be avoided as much as possible during the casting process. As such, steelmakers have been investing in research, with the aim of understanding better the phenomena leading to casting problems, and improve the processes when possible.

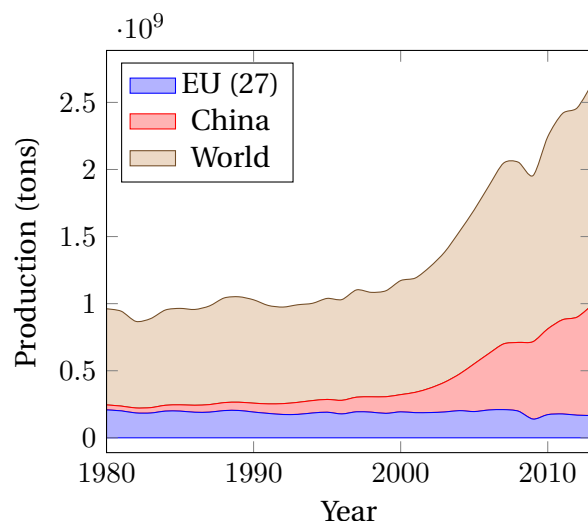


Fig. 1.8 – Evolution curves of crude steel worldwide production from 1980 to 2013 [WSA 2014].

Simulation software dedicated to alloy casting is one of the main research investments undertaken by steelmakers. These tools coming from academic research are actively used to optimize the process. However, few are the tools that take into account

the casting environment. For instance, the continuous casting process, in [fig. 1.7](#), is a chain process where the last steps involve rolls, water sprays and other components. A dedicated software is one that can provide the geometric requirements with suitable meshing capabilities, as well as respond to metallurgical and mechanical requirements, mainly by handling:

- moulds and their interaction with the alloy (thermal resistances ...)
- alloy filling and predicting velocity in the liquid and mushy zone
- thermomechanical stresses in the solid
- multicomponent alloys and predicting macrosegregation
- microstructure and phases
- finite solute diffusion in solid phases
- real alloy properties (not just constant thermophysical/thermomechanical properties)

1.5 Project context and objectives

1.5.1 Context

The European Space Agency (ESA) has been actively committed, since its foundation in 1975, in the research field. Its covers not only exclusive space applications, but also fundamental science like solidification. This thesis takes part in the ESA project entitled *CCEMLCC*, abbreviating "Chill Cooling for the Electro-Magnetic Levitator in relation with Continuous Casting of steel". The three-year contract from 2011 to late 2014 denoted *CCEMLCC II*, was preceded by an initial project phase, *CCEMLCC I*, from 2007 to 2009. The main focus is studying containerless solidification of steel under microgravity conditions. A chill plate is used to extract heat from the alloy, simulating the contact effect with a mould in continuous casting or ingot casting. A partnership of 7 industrial and academic entities was formed in *CCEMLCC II*. Here is a brief summary of each partner's commitment:

Academic partners

- Center for Material Forming (CEMEF) - France: numerical modelling of microgravity chill cooling experiments
- Deutsches Zentrum für Luft- und Raumfahrt (DLR or German Aerospace Centre) and Ruhr Universität Bochum (RUB) university - Germany: preparation of a chill cooling device for electromagnetic levitation (EML), microgravity testing and investigation of growth kinetics in chill-cooled and undercooled steel alloys

Chapter 1. General Introduction

- University of Alberta - Canada: impulse atomization and spray deposition of the D2 tool steel
- University of Bremen - Institut für Werkstofftechnik (IWT) institute - Germany: study of D2 tool steel melt solidification in atomization processing

Industrial partners

- ARCELORMITTAL (France): elaboration of a series of steel grades used in microgravity and ground-based studies
- METSO Minerals Inc. (Finland): material production with D2 tool steel for spray forming
- TRANSVALOR (France): development and marketing of the casting simulation software *Thercast[®]*

CEMEF, as an academic partner, contributed to the work by proposing numerical models in view of predicting the chill cooling of steel droplets. A first model was developed by [Rivaux \[2011\]](#). The experimental work by DLR considered various facilities and environments to set a droplet of molten alloy in levitation: EML ([fig. 1.9](#)) for ground-based experiments, microgravity during parabolic flight or sounding rockets and last, microgravity condition on-board the International Space Station (ISS).



Fig. 1.9 – Electromagnetic levitation [DLR 2014].

1.5.2 Objectives and outline

The main focus of the present thesis is predicting macrosegregation with liquid dynamics assuming a fixed solid phase, i.e. no account of solid transport (e.g. equiaxed crystals sedimentation) and no account of solid deformation. At CEMEF, this scope has been adopted in previous studies by [Gouttebroze \[2005\]](#), [Liu \[2005\]](#), [Mosbah \[2008\]](#), [Rivaux \[2011\]](#), and [Carozzani \[2012\]](#). Nevertheless, many modelling features evolved with time such as going from two-dimensional to three-dimensional modelling, resolution schemes for each of the conservation equations: energy, chemical species and liquid momentum, Eulerian or Lagrangian descriptions, modelling of grain structure and others. In this thesis, we propose a numerical model that takes into account i) the energy conservation in a temperature formulation based on a thermodynamic

1.5. Project context and objectives

database mapping, ii) the liquid momentum conservation with thermosolutal convection and solidification shrinkage as driving forces, iii) solute mass conservation with solidification shrinkage (to predict inverse segregation) and iv) solidification paths at full equilibrium for multicomponent alloys. Moreover, all equations are formulated in a pure Eulerian description while using the Level Set method to keep implicitly track of the interface between the alloy and the surrounding gas. To the author's knowledge, this work combining macrosegregation prediction using the level set methodology to track the metal-air interface during shrinkage has no precedent in casting and solidification literature. The model couples in a weak fashion, all four conservation equations presented in [fig. 1.10](#), showing on the one hand, that microsegregation is an essential common link between these equations, while on the other hand, the level set interacts with conservations equations by giving the interface position.

Numerical tools: Cimlib relying on PETSc, parallelised with MPICH2, paraview and python as tools for postprocess and analysis.

The previously mentionned simulation requirements are not met in a single casting software package. Nevertheless, *Thercast®* is a promising tool that already handles a part of the above points. The current thesis developments are done using C++ language as a part of the in-house code, known as *CimLib* [[Digonnet et al. 2007](#); [Mesri et al. 2009](#)]. This fully parallel library is the main academic research support for *Thercast®*

Outline: each chapter content ...

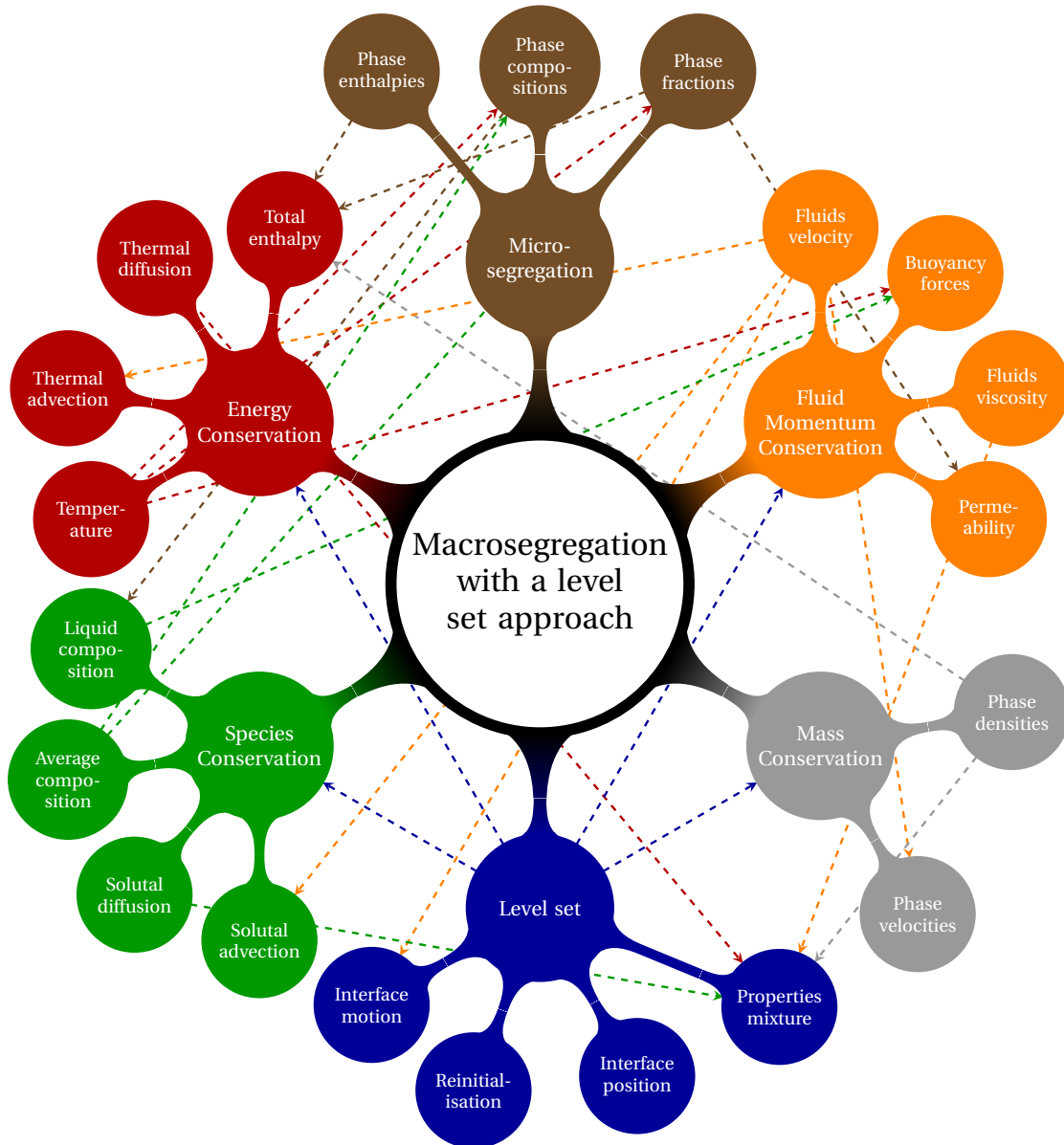


Fig. 1.10 – A graphical representation of the main ingredients of the numerical approach, for a macrosegregation model with the level set methodology, when no solid deformation or movement are considered. The dashed lines represent the possible interaction between the components.

Chapter 2

Modelling Review

Contents

2.1	Modelling macrosegregation	16
2.1.1	Macroscopic solidification model: monodomain	17
2.2	Eulerian and Lagrangian motion description	23
2.2.1	Overview	23
2.2.2	Interface capturing	25
2.3	Solidification models with level set	25
2.4	The level set method	26
2.4.1	Diffuse interface	27
2.4.2	Mixing Laws	28
2.5	Interface motion	30
2.5.1	Level set transport	31
2.5.2	Level set regularisation	32

2.1 Modelling macrosegregation

Microsegregation models

Solid formation depends greatly on the ability of chemicals species to diffuse within each of the solid and liquid phases, but also across the solid-liquid interface. Furthermore, chemical diffusion like all other diffusional processes, is a time-dependent phenomenon. One can thus conclude that two factors influence the amount of solid formation: cooling rate and diffusion coefficients. However, convection and other mechanical mixing sources, homogenise the composition much faster than atomic diffusion. As such, *complete mixing* in the liquid is always an acceptable assumption, regardless of the solidification time. We may speak of infinite diffusion in the liquid. Nevertheless, diffusion in the solid, also known as *back diffusion*, is the only transport mechanism with very low diffusion coefficients. Therefore, chemical species require a long time, i.e. low cooling rate, to completely diffuse within the solid. The difference in diffusional behaviour at the scale of a secondary dendrite arm, is summarized by two limiting segregation models of perfect equilibrium and nonequilibrium, which are the lever rule and Gulliver-Scheil models, respectively. Afterwards, models with finite back diffusion are presented.

Lever rule

The lever rule considers an ideal equilibrium in all phases, i.e. solidification is extremely slow, hence phase compositions are homogeneous ($w^{l*} = w^l$ and $w^{s*} = w^s$) at all times as a consequence of complete mixing. These compositions are given by:

$$w^l = w^{l*} = k^{-1}w^{s*} = k^{-1}w^s \quad (2.1)$$

$$w^s = w^{s*} = \frac{kw_0}{kf^s + (1 - f^s)} \quad (2.2)$$

At the end of solidification, the composition of the solid phase is equal to the nominal composition, $w^s = w_0$

Gulliver-Scheil

The other limiting case is the absence of diffusion in the solid. That includes also the diffusion at the interface, so nothing diffuses in or out. The consequence is a steady increase of the homogeneous liquid composition while the solid composition remains non-uniform. Compared to a full equilibrium approach, higher fractions of liquid will remain until eutectic composition is reached, triggering a eutectic solidification. The

phase compositions are given by:

$$w^l = w^{l*} = k^{-1} w^{s*} \quad (2.3)$$

$$w^{s*} = kw_0(1 - f^s)^{k-1} \quad (2.4)$$

Finite back diffusion

It has been concluded that the assumption of a negligable back diffusion overestimates the liquid composition and the resulting eutectic fraction. Therefore, many models studied the limited diffusion in the solid. One of the earliest models is the Brody-Flemings models [Khan et al. 2014] that is a based on a differential solute balance equation for a parabolic growth rate, as follows:

$$w^l = w^{l*} = k^{-1} w^{s*} \quad (2.5)$$

$$w^{s*} = kw_0 [1 - (1 - 2\text{Fo}^s k) f^s]^{\frac{k-1}{1-2\text{Fo}^s k}} \quad (2.6)$$

where Fo^s is the dimensionless *Fourier number* for diffusion in the solid [Dantzig et al. 2009]. It depends on the solid diffusion coefficient D^s , solidification time t_s and the secondary dendrite arm spacing, as follows:

$$\text{Fo}^s = \frac{D^s t_s}{(\lambda_2/2)^2} \quad (2.7)$$

Several other models were since suggested and used. The interested reader is referred to the following non exhaustive list of publications: Clyne et al. [1981], Kobayashi [1988], Ni et al. [1991], Wang et al. [1993], Combeau et al. [1996], Martorano et al. [2003], and Tourret et al. [2009]. It is noted that some of these publications consider also a finite diffusion in the liquid phase.

2.1.1 Macroscopic solidification model: monodomain

In this section, we will present the macroscopic conservations equations that enable us to predict macrosegregation in the metal when the latter is the only domain in the system.

Volume averaging

It is crucial for a solidification model to represent phenomena on the microscale, then scale up to predict macrscopic phenomena. Nevertheless, the characteristic length of a small scale in solidification may represent a dendrite arm spacing, for instance the mushy zone permeability, as it may also represent an atomic distance if one is interested, for instance, in the growth competition between diffusion and surface

energy of the solid-liquid interface. Modelling infinitely small-scale phenomena could be prohibitively expensive in computation time, if we target industrial scales.

The volume averaging is a technique that allows bypassing this barrier by averaging small-scale variations on a so-called *representative volume element* (RVE) [Dantzig et al. 2009] of volume V_E , with the following dimensional constraints: the element should be large enough to "see" and average microscopic fluctuations whilst being smaller than the scale of macroscopic variations. Solid and liquid may exist simultaneously in the RVE, but no gas phase is considered (volume saturation: $V^s + V^l = V_E$). Moreover, temperature is assumed uniform and equal for all the phases. The formalism, introduced by Ni et al. [1991], is summarized by the following equations for any physical quantity ψ :

$$\langle \psi \rangle = \frac{1}{V_E} \int_{V_E} \psi \, d\Omega = \langle \psi^s \rangle + \langle \psi^l \rangle \quad (2.8)$$

where $\langle \psi \rangle^s$ and $\langle \psi \rangle^l$ are phase averages of ψ . Then, for any phase ϕ , one can introduce the *phase intrinsic average* of ψ , denoted $\langle \psi \rangle^\phi$, by writing:

$$\langle \psi^\phi \rangle = \frac{1}{V_E} \int_{V_\phi} \psi \, d\Omega = g^\phi \langle \psi \rangle^\phi \quad (2.9)$$

where g^ϕ is the volume fraction of phase ϕ with $g^\phi = V_\phi/V_E$. To finalize, the averaging is applied to temporal and spatial derivation operators:

$$\langle \frac{\partial \psi^\phi}{\partial t} \rangle = \frac{\partial \langle \psi^\phi \rangle}{\partial t} - \int_{\Gamma^*} \psi^\phi \vec{v}^* \cdot \vec{n}^\phi \, dA \quad (2.10)$$

$$\langle \vec{\nabla} \psi^\phi \rangle = \vec{\nabla} \langle \psi^\phi \rangle + \int_{\Gamma^*} \psi^\phi \vec{n}^\phi \, dA \quad (2.11)$$

where \vec{v}^* is the local relative interface velocity and Γ^* is the solid-liquid interface, while n^ϕ is the normal to Γ^* , directed outwards. The surface integral terms in eqs. (2.10) and (2.11) are *interfacial averages* that express exchanges between the phases across the interface. The previous equations will be used to derive a set macroscopic conservation equations. It is noted that the intrinsic average $\langle \psi \rangle^\phi$ may be replaced by ψ^ϕ for notation simplicity, whenever the averaging technique applies.

Macroscopic equations

A monodomain macroscopic model relies on four main conservation equations to predict macrosegregation in a single alloy, i.e. the latter is considered without any interaction with another alloy or ambient air. The general form of an averaged conser-

2.1. Modelling macrosegregation

vation equation of any physical quantity ψ is given by:

$$\frac{\partial \langle \psi \rangle}{\partial t} + \nabla \cdot \langle \psi \vec{v} \rangle + \nabla \cdot \langle \vec{j}_\psi \rangle = \langle Q_\psi \rangle \quad (2.12)$$

The first LHS term in eq. (2.12) represents the time variation of ψ , the second term accounts for transport by advection while the third is the diffusive transport and the RHS term represents a volume source. The considered equations are mass, energy, species conservation and momentum, all summarized in table 2.1. The latter equation is averaged only for the liquid phase, as we assume a fixed and rigid solid phase ($\vec{v}^s = \vec{0}$), thus the corresponding equation vanishes. We develop the ingredients of these

Table 2.1 – Summary of conservation equations with their variables.

Conservation Equation	ψ	\vec{j}_ψ	Q_ψ
Mass	ρ	—	—
Energy	ρh	\vec{q}	—
Species	ρw_i	\vec{j}_i	—
Liquid momentum	$\rho^l \vec{v}^l$	$-\overline{\sigma^l}$	\vec{F}_v^l

equations using the averaging technique, as follows:

$$\langle \rho \rangle = g^l \rho^l + g^s \rho^s \quad (2.13)$$

$$\langle \rho \vec{v} \rangle = g^l \rho^l \vec{v}^l + g^s \rho^s \vec{v}^s \quad (2.14)$$

$$\langle \rho h \rangle = g^l \rho^l h^l + g^s \rho^s h^s \quad (2.15)$$

$$\langle \rho h \vec{v} \rangle = g^l \rho^l h^l \vec{v}^l + g^s \rho^s h^s \vec{v}^s \quad (2.16)$$

$$\langle \rho w_i \rangle = g^l \rho^l w_i^l + g^s \rho^s w_i^s \quad (2.17)$$

$$\langle \rho w_i \vec{v} \rangle = g^l \rho^l w_i^l \vec{v}^l + g^s \rho^s w_i^s \vec{v}^s \quad (2.18)$$

$$\langle \rho^l \vec{v}^l \rangle = \langle \rho^l \vec{v}^l \rangle^l = g^l \rho^l \vec{v}^l \quad (2.19)$$

$$\langle \rho^l \vec{v}^l \times \vec{v} \rangle = g^l \rho^l \vec{v}^l \times \vec{v}^l + g^s \rho^s \vec{v}^l \times \vec{v}^s \quad (2.20)$$

Next, we define the average diffusive fluxes, \vec{q} for energy and \vec{j}_i for solutes, using Fourier's conduction law and Fick's first law, respectively [Rappaz et al. 2003]:

$$\langle \vec{q} \rangle = -g^l \langle \kappa^l \rangle \vec{\nabla} T - g^s \langle \kappa^s \rangle \vec{\nabla} T = -\langle \kappa \rangle \vec{\nabla} T \quad (2.21)$$

$$\langle \vec{j}_i \rangle = -g^l \rho^l D^l \vec{\nabla} w_i^l - g^s \rho^s D^s \vec{\nabla} w_i^s \quad (2.22)$$

In eq. (2.22), the macroscopic diffusion coefficient in the solid is neglected, by considering that for macroscopic scales, the average composition of the alloy is much more influenced by advective and diffusive transport in the liquid. In eq. (2.21), we assume

Chapter 2. Modelling Review

that phases are at thermal equilibrium, that is, temperature is uniform in the RVE.

Now that the main conservation equations ingredients are properly defined, we may write each averaged conservation equation as the sum of two local conservation equations for each phase in the RVE, hence introducing also interfacial average terms. For instance, the local mass balance in each phase is given by:

$$\frac{\partial}{\partial t} \left(g^l \rho^l \right) + \nabla \cdot \left(g^l \rho^l \vec{v}^l \right) = S_V \langle \rho^l \vec{v}^{l*} \cdot \vec{n} \rangle^* - S_V \langle \rho^l \vec{v}^* \cdot \vec{n} \rangle^* \quad (2.23a)$$

$$\frac{\partial}{\partial t} \left(g^s \rho^s \right) + \nabla \cdot \left(g^s \rho^s \vec{v}^s \right) = -S_V \langle \rho^s \vec{v}^{s*} \cdot \vec{n} \rangle^* + S_V \langle \rho^s \vec{v}^* \cdot \vec{n} \rangle^* \quad (2.23b)$$

where $S_V = A_{sl}/V_E$ is the specific surface area, \vec{v}^{l*} and \vec{v}^{s*} are respectively, the liquid and solid phase velocity at the interface and \vec{v}^* is the previously introduced solid-liquid interface velocity. For instance, the first interfacial exchange term in the RHS of eq. (2.23a) is expanded as follows [Dantzig et al. 2009]:

$$S_V \langle \rho^l \vec{v}^{l*} \cdot \vec{n} \rangle^* = \frac{A_{sl}}{V_E} \left(\frac{1}{A_{sl}} \int_{A_{sl}} \rho^l \vec{v}^{l*} \cdot \vec{n} \, dA \right) \quad (2.24a)$$

$$= \frac{1}{V_E} \int_{A_{sl}} \rho^l \vec{v}^{l*} \cdot \vec{n} \, dA \quad (2.24b)$$

Summing equations (2.23a) and (2.23b), results in the overall mass balance in the RVE:

$$\begin{aligned} \frac{\partial}{\partial t} \left(g^l \rho^l + g^s \rho^s \right) + \nabla \cdot \left(g^l \rho^l \vec{v}^l + g^s \rho^s \vec{v}^s \right) = \\ S_V \langle \rho^l \left(\vec{v}^{l*} - \vec{v}^* \right) \cdot \vec{n} \rangle^* - S_V \langle \rho^s \left(\vec{v}^{s*} - \vec{v}^* \right) \cdot \vec{n} \rangle^* \end{aligned} \quad (2.25)$$

where the RHS cancels to zero as shown by Ni et al. [1991]. Moreover, the authors show that with their averaging technique, interfacial exchanges for energy, chemical species and momentum cancel out as they are equal in absolute value but opposite in sign. Using eqs. (2.13) to (2.22) and following the same procedure done in eq. (2.25), the averaged mass balance hence writes:

$$\frac{\partial \langle \rho \rangle}{\partial t} + \nabla \cdot \langle \rho \vec{v} \rangle = 0 \quad (2.26)$$

whereas the averaged energy balance writes:

$$\frac{\partial \langle \rho h \rangle}{\partial t} + \nabla \cdot \langle \rho h \vec{v} \rangle - \nabla \cdot \left(\langle \kappa \rangle \vec{\nabla} T \right) = 0 \quad (2.27)$$

and finally the species balance writes:

$$\frac{\partial \langle \rho w_i \rangle}{\partial t} + \nabla \cdot \langle \rho w_i \vec{v} \rangle - \nabla \cdot \left(g^l \rho^l D^l \vec{\nabla} w_i^l \right) = 0 \quad (2.28)$$

As stated previously, the momentum balance in the solid phase is not taken into consideration, hence we do not sum the corresponding local conservation equations. This has consequences on the advection terms in energy and species conservation, and later on we will show the consequences on the momentum conservation in the liquid. First, the advection terms in [eqs. \(2.27\)](#) and [\(2.28\)](#) shall be redefined by considering that the fluid is incompressible ($\nabla \cdot \langle \vec{v}^l \rangle = 0$), which yields:

$$\nabla \cdot \langle \rho h \vec{v} \rangle = \langle \vec{v}^l \rangle \cdot \vec{\nabla} (\rho^l h^l) \quad (2.29)$$

$$\nabla \cdot \langle \rho w_i \vec{v} \rangle = \langle \vec{v}^l \rangle \cdot \vec{\nabla} (\rho^l w_i^l) \quad (2.30)$$

As for the liquid momentum balance, we write:

$$\frac{\partial}{\partial t} (\rho^l g^l \vec{v}^l) + \vec{\nabla} \cdot (\rho^l g^l \vec{v}^l \times \vec{v}^l) = \vec{\nabla} \cdot (g^l \vec{\sigma}^l) + g^l \vec{F}_v^l + \vec{\Gamma}^l \quad (2.31)$$

where \vec{F}_v^l is the vector of external body forces exerted on the liquid phase. In our case, it accounts for the fluid's weight:

$$\vec{F}_v^l = \rho^l \vec{g} \quad (2.32)$$

The interfacial momentum transfer between the solid and liquid phases in [eq. \(2.31\)](#) is modelled by a momentum flux vector $\vec{\Gamma}^l$, consisting of hydrostatic and deviatoric parts, such that:

$$\vec{\Gamma}^l = \vec{\Gamma}_p^l + \vec{\Gamma}_{\mathbb{S}}^l \quad (2.33)$$

$$\vec{\Gamma}_p^l = p^{l*} \vec{\nabla} g^l = p^l \vec{\nabla} g^l \quad (2.34)$$

$$\vec{\Gamma}_{\mathbb{S}}^l = -g^{l2} \mu^l \mathbb{K}^{-1} (\vec{v}^l - \vec{x}^s) \quad (2.35)$$

where p^{l*} is the pressure at the interface, considered to be equal to the liquid hydrostatic pressure p^l , \mathbb{K} is a permeability scalar (isotropic) computed using [eq. \(1.2\)](#) and μ^l is the liquid's dynamic viscosity. The general form of the Cauchy liquid stress tensor in [eq. \(2.31\)](#) is decomposed as follows:

$$\langle \bar{\bar{\sigma}}^l \rangle = g^l \bar{\bar{\sigma}}^l = -(\langle p^l \rangle - \lambda \nabla \cdot \langle \vec{v}^l \rangle) \bar{\bar{I}} + \langle \bar{\bar{\mathbb{S}}}^l \rangle \quad (2.36)$$

where λ is a dilatational viscosity [[Dantzig et al. 2009](#)] and $\bar{\bar{\mathbb{S}}}^l$ is the liquid strain deviator tensor. In the literature, the coefficient λ is taken proportional to the viscosity: $\lambda = \frac{2}{3} \mu^l$. However, as we consider an incompressible flow, the divergence term vanishes, thus

rewriting eq. (2.36) as follows:

$$\langle \bar{\bar{\sigma}}^l \rangle = -\langle p^l \rangle \bar{\bar{I}} + \langle \bar{\bar{S}}^l \rangle \quad (2.37a)$$

$$\langle \bar{\bar{\sigma}}^l \rangle = -\langle p^l \rangle \bar{\bar{I}} + 2\mu^l \langle \dot{\bar{\bar{\varepsilon}}}^l \rangle \quad (2.37b)$$

where the transition from eq. (2.37a) to eq. (2.37b) is made possible by assuming a Newtonian behaviour for the liquid phase. The strain rate tensor, $\langle \dot{\bar{\bar{\varepsilon}}}^l \rangle$, depends on the average liquid velocity:

$$\langle \dot{\bar{\bar{\varepsilon}}}^l \rangle = \frac{1}{2} \left(\bar{\bar{\nabla}} \langle \vec{v}^l \rangle + \bar{\bar{\nabla}}^t \langle \vec{v}^l \rangle \right) \quad (2.38)$$

Finally, we obtain the final form of momentum conservation in the liquid phase coupled with the averaged mass balance, by injecting eqs. (2.32), (2.34), (2.35), (2.37b) and (2.38) in eq. (2.31):

$$\begin{aligned} \frac{\partial}{\partial t} \left(\rho^l \langle \vec{v}^l \rangle \right) + \frac{1}{g^l} \vec{\nabla} \cdot \left(\rho^l \langle \vec{v}^l \rangle \times \langle \vec{v}^l \rangle \right) = \\ - g^l \vec{\nabla} p^l - 2\mu^l \vec{\nabla} \cdot \left(\bar{\bar{\nabla}} \langle \vec{v}^l \rangle + \bar{\bar{\nabla}}^t \langle \vec{v}^l \rangle \right) - g^l \mu^l \mathbb{K}^{-1} \langle \vec{v}^l \rangle + g^l \rho^l \vec{g} \end{aligned} \quad (2.39)$$

where we intentionally employed the *superficial velocity*, $\langle \vec{v}^l \rangle = g^l \vec{v}^l$, as the main unknown, together with the liquid pressure p^l . This system, when modelled in 3D, has a total of 4 unknowns (velocity vector and pressure) and 3 equations (X, Y and Z projections for the velocity vector). A fourth equation provided by the mass balance (eq. (2.26)) is therefore added for closure, giving the following system of equations :

$$\left\{ \begin{array}{l} \frac{\partial}{\partial t} \left(\rho^l \langle \vec{v}^l \rangle \right) + \frac{1}{g^l} \vec{\nabla} \cdot \left(\rho^l \langle \vec{v}^l \rangle \times \langle \vec{v}^l \rangle \right) = \\ - g^l \vec{\nabla} p^l - 2\mu^l \vec{\nabla} \cdot \left(\bar{\bar{\nabla}} \langle \vec{v}^l \rangle + \bar{\bar{\nabla}}^t \langle \vec{v}^l \rangle \right) - g^l \mu^l \mathbb{K}^{-1} \langle \vec{v}^l \rangle + g^l \rho^l \vec{g} \\ \nabla \cdot \langle \vec{v}^l \rangle = 0 \end{array} \right. \quad (2.40)$$

Last, the Boussinesq approximation allows taking a constant density in the inertial terms of eq. (2.40) while the variations responsible for buoyancy forces can be computed using ??, if the system is incompressible. Hence, the final set of equations is better known as the incompressible *Navier-Stokes* equations, applied to a solidifying

2.2. Eulerian and Lagrangian motion description

melt:

$$\left\{ \begin{array}{l} \rho_0^l \left(\frac{\partial \langle \vec{v}^l \rangle}{\partial t} + \frac{1}{g^l} \vec{\nabla} \cdot (\langle \vec{v}^l \rangle \times \langle \vec{v}^l \rangle) \right) = \\ - g^l \vec{\nabla} p^l - 2\mu^l \vec{\nabla} \cdot (\overline{\vec{\nabla}} \langle \vec{v}^l \rangle + \overline{\vec{\nabla}}^t \langle \vec{v}^l \rangle) - g^l \mu^l \mathbb{K}^{-1} \langle \vec{v}^l \rangle + g^l \rho^l \vec{g} \\ \nabla \cdot \langle \vec{v}^l \rangle = 0 \end{array} \right. \quad (2.41)$$

Since all conservation equations were presented and simplified by the main assumption of a static solid phase, we may include them in a graphical summary in [section 2.1.1](#)

* Macro models: Rivaux ? Gu beckermann 1999 ?

* Micro macro: Tommy Carozzani2013, guo beckermann 2003, Combeau 2009, Miha Zaloznik 2010 (indirect), P. Thévoz, J.-L. Desbiolles, M. Rappaz, Metallurgical and Materials TransactionsA 20 (2) (1989) 311–322

* end by talking about taking air into account and the need for an interface capturing method

2.2 Eulerian and Lagrangian motion description

2.2.1 Overview

In mechanics, it is possible to describe motion using two well-known motion description: Eulerian and Lagrangian descriptions. To start with the latter, it describes the motion of a particle by attributing a reference frame that moves with the particle. In other words, the particle itself is the center of a reference frame moving at the same speed during time. The position vector, denoted by \vec{x} , is hence updated as follows:

$$\vec{x}^{(t+1)} = \vec{x}^{(t)} + \vec{v} \Delta t \quad (2.45)$$

As such, the total variation of any physical quantity ψ related to the particle can be found by deriving with respect to time, $\frac{d\psi}{dt}$. In contrast to the Lagrangian description, the Eulerian description considers a fixed reference frame and independent of the particle's trajectory. The total variation of ψ cannot be simply described by a temporal derivative, since the particle's velocity is not known to the reference frame, and thus the velocity effect, namely the advective transport of ψ , should also be considered as follows:

$$\frac{d\psi}{dt} = \frac{\partial \psi}{\partial t} + \underbrace{\vec{v} \cdot \vec{\nabla} \psi}_{\substack{\text{Advection} \\ \text{Transport}}} \quad (2.46)$$

In this case, the LHS term is also known as *total* or *material derivative*. The importance of these motion descriptions is essential to solve mechanics, whether for fluids or

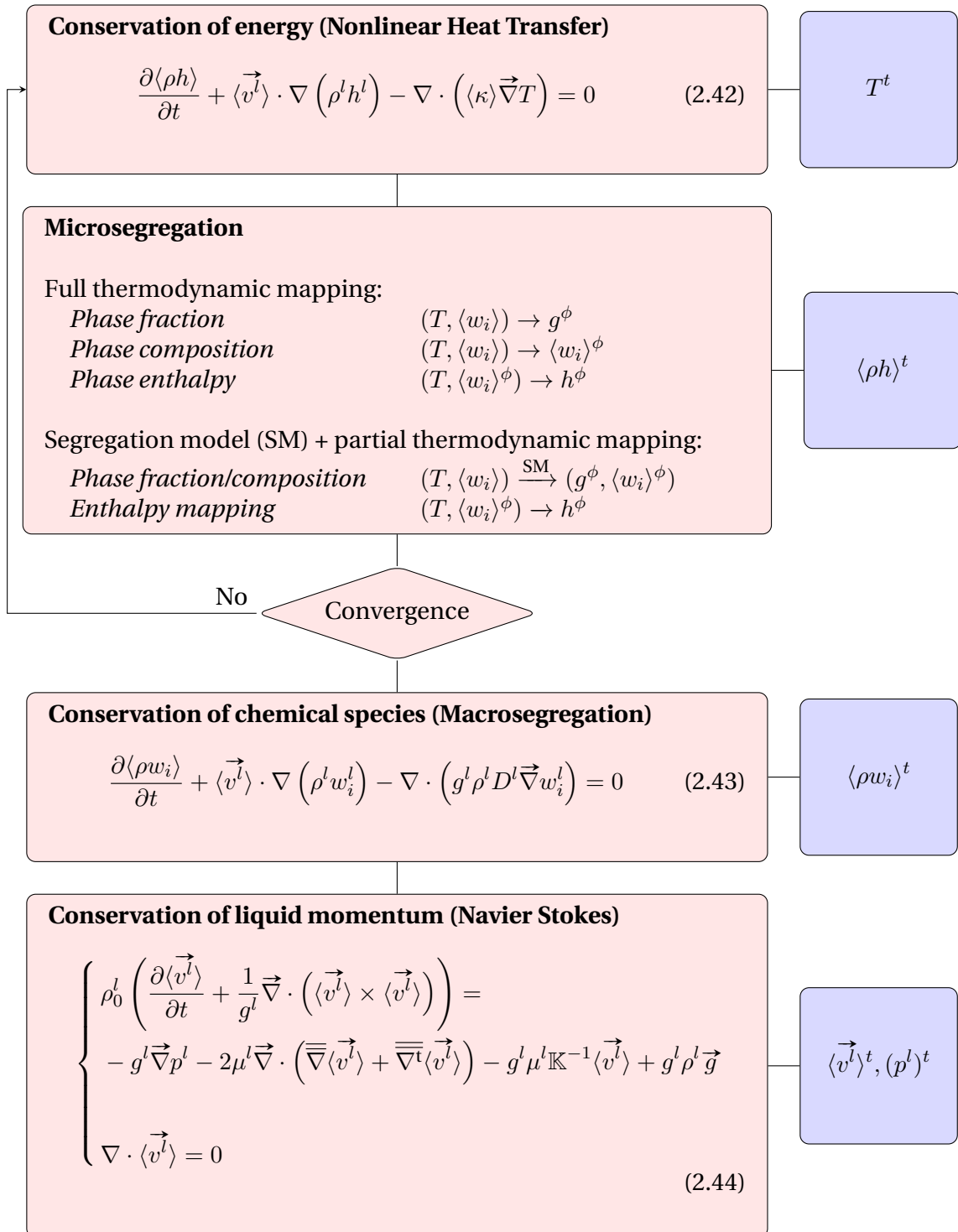


Fig. 2.1 – Graphical resolution algorithm of the conservation equations used in a monodomain macroscopic model to predict macrosegregation for a time increment t . The blue boxes represent the output of each equation.

solids, using a numerical method like the finite element method (FEM). One of the main steps of this method is to spatially discretise a continuum into a grid of points (nodes, vertices ...), where any physical field shall be accordingly discretised. Now, if we focus on a node where velocity has a non zero value and following the previously made analysis, two outcomes are possible: either the node would be fixed (Eulerian) or it would move by a distance proportional to the prescribed velocity (Lagrangian). In the latter case, points located on the boundaries constantly require an update of the imposed boundary conditions.

From these explanations, one can deduce that an Eulerian framework is suited for fluid mechanics problems where velocities are high and may distort the mesh points, whereas the Lagrangian framework is better suited for solid mechanics problems where deformation velocities are relatively low and should well behave when predicting strains.

Another motion description has emerged some decades ago, [Hirt \[1971\]](#) call it the Arbitrary Langrangian-Eulerian (ALE) method. ALE combines advantages from both previous descriptions as it dictates a Lagrangian behaviour at "solid" nodes where solid is deforming, and an Eulerian behaviour at "fluid" nodes.

2.2.2 Interface capturing

As no solid deformation is considered in this work, the Eulerian framework is a convenient choice. Solidification shrinkage is to be considered in our current scope, so it will deform the alloy's outer surface in contact with the air. We intend to track this interface and its motion over time via a numerical method. A wide variety of methods accomplish this task while they yield different advantages and disadvantages. Such methods fall into two main classes, either interface tracking or interface capturing, among which we cite: marker-and-cell (MAC) [[Harlow et al. 1965](#)], volume of fluid (VOF) [[Hirt et al. 1981](#)], phase field methods (PF), level set method (LSM) [[Osher et al. 1988](#)], coupled level set - VOF method and others. The interested reader may refer to quick references by [Prosperetti \[2002\]](#) and [Maitre \[2006\]](#) about these methods.

In the past years, the level set method received a considerable attention in many computational fields, specifically in solidification. For this reason, we will focus on this method henceforth, giving a brief literature review and technical details in the next sections.

2.3 Solidification models with level set

In classic solidification problems, the need to track an interface occurs usually at the solid-liquid interface, that is why the phase field method [[Karma et al. 1996; Boettinger et al. 2002](#)] and the level set method [[Chen et al. 1997; Gibou et al. 2003; Tan et al. 2003](#)]

2007] were applied at a microscale to follow mainly the dendritic growth of a single crystal in an undercooled melt. In our case however, when we mention "solidification models using LSM", we do not mean the solid-liquid interface inside the alloy, but it is the alloy(liquid)-air interface that we intend to track, assuming that microscale phenomena between the phases within the alloy, are averaged using the previously defined technique in [section 2.1.1](#).

Very few models were found in the literature, combining solidification and level set as stated previously. [Du et al. \[2001\]](#) applied it to track the interface between two molten alloys in a double casting technique. Welding research, on another hand, has been more active adapting the level set methodology to corresponding applications. In CEMEF, two projects made use of the metal-air level set methodology in welding simulations and showed promising results. [Desmaison et al. \[2014\]](#) employed this methodology to simulate a hybrid arc and laser beam welding used in high thickness steel sheet welding. Later, [Chen \[2014\]](#) applied it to gas metal arc welding (GMAW) to predict the grain structure in the heat affected zone essentially. More recently, [Courtois et al. \[2014\]](#) used the same methodology but this time to predict keyhole defect formation in spot laser welding. The tracked interface in this case was that between the molten alloy and the corresponding vapor phase.

2.4 The level set method

Firstly introduced by [Osher et al. \[1988\]](#), this method became very popular in studying multiphase flows. It is reminded that the term *multiphase* in computational domains usually refers to multiple fluids, and thus should not be mixed with definition of a phase in the current solidification context. For disambiguation, we shall use *multifluid flow* when needed. The great advantage lies in the way the interface between two fluids, F_1 and F_2 is implicitly captured, unlike other methods where the exact interface position is needed. In a discrete domain, the concept is to assign for each mesh node of position vector \vec{x} , the minimum distance $d_\Gamma(\vec{x})$ separating it from an interface Γ . The distance function, denoted α and defined in [eq. \(2.47\)](#), is then signed positive or negative, based on the fluid or domain to which the node belongs.

$$\alpha(\vec{x}) = \begin{cases} d_\Gamma(\vec{x}) & \text{if } \vec{x} \in F_1 \\ -d_\Gamma(\vec{x}) & \text{if } \vec{x} \in F_2 \\ 0 & \text{if } \vec{x} \in \Gamma_{F1,F2} \end{cases} \quad (2.47)$$

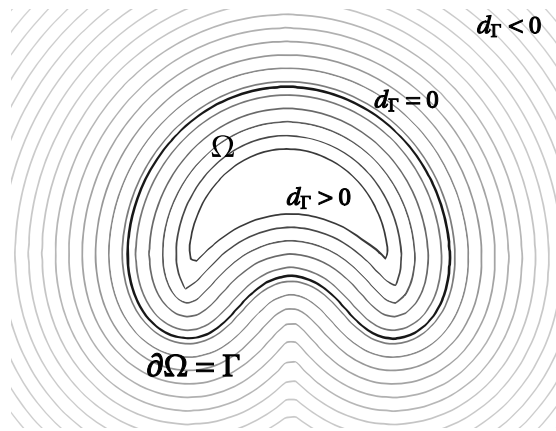


Fig. 2.2 – Schematic of the interface Γ (thick black line) of a rising air bubble (Ω) in water. The other contours represent isovalues of the distance function around and inside the interface contour. Those outside are signed negative whereas inside they are signed positive.

2.4.1 Diffuse interface

The level set has many attractive properties that allows seamless implementation in 2D and 3D models. It is a continuously differentiable C^1 -function. The Heaviside function is also continuous but non differentiable, with an abrupt transition from 0 to 1 across the sharp interface, as follows:

$$H = H(\alpha(\vec{x})) = \begin{cases} 0 & \text{if } \alpha(\vec{x}) < 0 \\ 1 & \text{if } \alpha(\vec{x}) \geq 0 \end{cases} \quad (2.48)$$

With the help of eq. (2.48), we can define the geometric "presence" of a domain with respect to the interface. As such, material properties depend upon this function, which will be discussed later in section 2.4.2. It is established that a steep transition can lead to numerical problems, so the Heaviside function should be smoothed in a volume of fixed thickness around the interface. Sinusoidal smoothing in eq. (2.49) is widely used with level set formulations.

$$H = \begin{cases} 0 & \text{if } \alpha(\vec{x}) < -\varepsilon \\ 1 & \text{if } \alpha(\vec{x}) > \varepsilon \\ \frac{1}{2} \left(1 + \frac{\alpha(\vec{x})}{\varepsilon} + \frac{1}{\pi} \sin \left(\frac{\pi \alpha(\vec{x})}{\varepsilon} \right) \right) & \text{if } -\varepsilon \leq \alpha(\vec{x}) \leq \varepsilon \end{cases} \quad (2.49)$$

where the interval $[-\varepsilon; +\varepsilon]$ is an artificial interface thickness around the zero distance. Defining a diffuse interface rather than a sharp one, is also a common approach in phase field methods [Beckermann et al. 1999; Sun et al. 2004]. It is emphasized that the latter methods give physically meaningful analysis of a diffuse interface and the optimal thickness by thoroughly studying the intricate phenomena happening at the

scale of the interface. However, for level set methods, there has not been a formal work leading the same type of analysis. For this reason, many aspects of the level set method lack physical meanings but remain computationally useful. In a recent paper by [Gada et al. \[2009\]](#), the authors respond partially to this problem by analysing and deriving conservation equations using a level set in a more meaningful way, but do not discuss the diffuse interface aspect.

The Dirac delta function is also an important property to convert surface integrals to volume terms, which could turn useful when modelling surface tension effects for instance, using the *continuum surface force* method (CSF) [[Brackbill et al. 1992](#)]. The Dirac function, plotted in [fig. 2.3](#) along with the Heaviside function within an interface thickness of $[-\varepsilon; +\varepsilon]$, is derived from the Heaviside as follows:

$$\delta(\alpha) = \delta(\alpha(\vec{x})) = \frac{\partial H}{\partial \alpha(\vec{x})} = \begin{cases} \frac{1}{2\varepsilon} \left(1 + \cos\left(\frac{\pi\alpha(\vec{x})}{\varepsilon}\right) \right) & \text{if } |\alpha(\vec{x})| \leq \varepsilon \\ 0 & \text{if } |\alpha(\vec{x})| > \varepsilon \end{cases} \quad (2.50)$$

The Heaviside and delta Dirac functions can be readily processed to obtain other geometric properties from the level set, which are extremely useful. We mention the most relevant ones [[Peng et al. 1999](#)]:

$$\text{normal vector : } \vec{n} = \frac{\vec{\nabla}\alpha}{\|\vec{\nabla}\alpha\|} \quad (2.51)$$

$$\text{curvature : } \zeta = -\nabla \cdot \vec{n} \quad (2.52)$$

$$\text{surface area of the air-metal interface : } A^\Gamma = \int_{\Omega} \delta(\alpha) \|\vec{\nabla}\alpha\| d\Omega \quad (2.53)$$

$$\text{metal volume : } V^M = \int_{\Omega} H^M d\Omega \quad (2.54)$$

where, for the last two equations, we consider a three-dimensional domain Ω containing two subdomains, metal and air, separated by an interface Γ . It is reminded that for a 2D case, [eq. \(2.53\)](#) evaluates a length instead of the area while [eq. \(2.54\)](#) gives the area instead of volume. Finally, within the diffuse interface, fluids properties may vary linearly or not, depending on the mixing law, which is presented in the next section.

2.4.2 Mixing Laws

A *monolithic* resolution style, as opposed to a *partitioned* resolution, is based on solving a single set of equations for both fluids separated by an interface, as if a single fluid were considered. Level set is one among many methods that use the monolithic style to derive a single set of conservation equations for both fluids. The switch from one material to the other is implicitly taken care of by using the Heaviside function as well as mixing laws. These laws are crucial to define how properties vary across

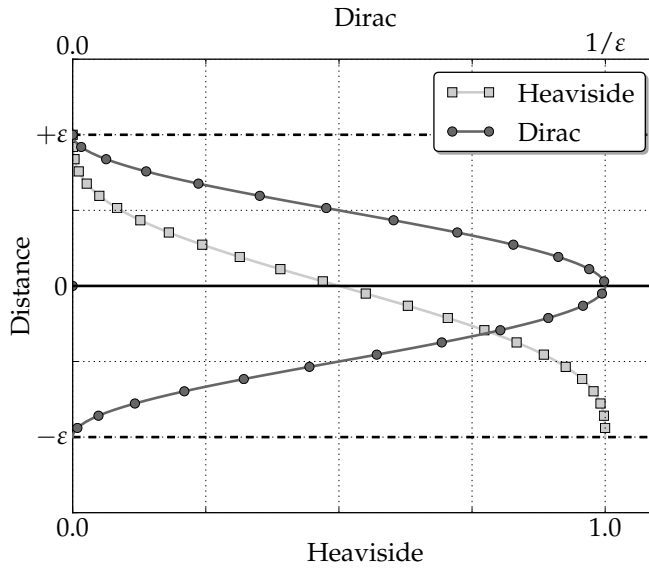


Fig. 2.3 – Schematic of two level properties inside the diffuse interface: Heaviside (lower x-axis) and Dirac delta (upper x-axis) functions. Note that the peak of the Dirac function depends on the interface thickness to ensure a unity integral of the delta function over Ω .

the diffuse interface in view of a more accurate resolution. The most frequently used mixing law in the literature is the arithmetic law. Other transitions are less known such as the harmonic and logarithmic mixing. The first law is maybe the most intuitive and most used for properties mixture as it emanates from VOF-based methods. If we consider any property ψ (for instance the fluid's dynamic viscosity μ) then the arithmetic law will give a mixed property $\hat{\psi}$ as follows:

$$\hat{\psi} = H^{F_1} \psi^{F_1} + H^{F_2} \psi^{F_2} \quad (2.55)$$

Basically, the result is an average property that follows the same trend as the Heaviside function. As for the harmonic law, it writes:

$$\hat{\psi} = \left(\frac{H^{F_1}}{\psi^{F_1}} + \frac{H^{F_2}}{\psi^{F_2}} \right)^{-1} \quad (2.56)$$

and last, the logarithmic law writes:

$$\hat{\psi} = n^{(H^{F_1} \log_n \psi^{F_1} + H^{F_2} \log_n \psi^{F_2})} \quad (2.57)$$

where n is any real number serving as a logarithm base, which often is either the exponential e or 10. The mixture result with this law is the same, regardless of the value of n . By looking to [fig. 2.4](#), we clearly see that the difference between all three approaches is the property weight given to each side of the level set in the mixture. The arithmetic law, being symmetric, has equal weights, ψ^{F_1} and ψ^{F_2} , in the final mixture.

Nevertheless, the asymmetric harmonic mixing varies inside the diffuse interface with a dominant weight of one property over the other. As for the logarithmic mixture, it can be seen as an intermediate transition between the preceding laws. As long

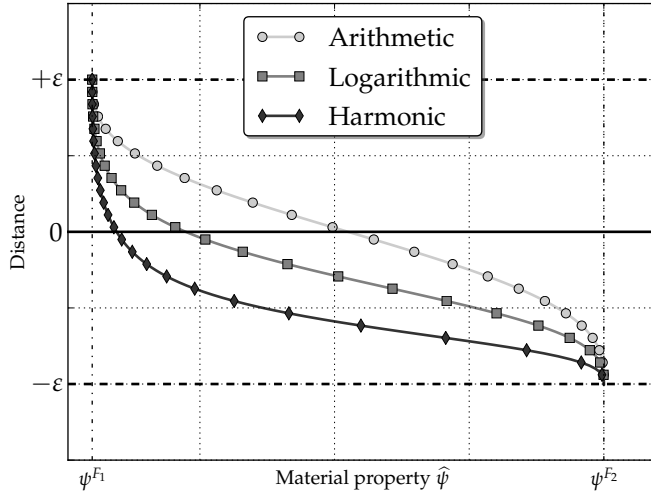


Fig. 2.4 – Three mixing laws, arithmetic, logarithmic and harmonic commonly used in monolithic formulations.

as the interface thickness is small enough, the choice of a mixing law should not drastically change the result, inasmuch as it depends on the discretisation resolution of the interface. This fact made the arithmetic mixing the most applied one, because it is symmetric and easy to implement (no handling of potential division problems like harmonic laws for instance). However, [Strotos et al. \[2008\]](#) claim that the harmonic law proves to conserve better diffusive fluxes at the interface. More recently, an interesting study made by [Ettrich et al. \[2014\]](#) focused on mixing thermal properties using a phase field method. They define a diffuse interface in which they separately mix the thermal conductivity, κ , and the heat capacity, C_p , then compute the thermal diffusivity as the ratio of these properties. Later, the authors compare the temperature field obtained by diffusion to a reference case in order to decide which combination of mixing laws gives the best result. Despite not being directly related to a level set method, this work gives an insight of the mixture possibilities and their effect on a pure thermal diffusion. Otherwise, little work has been found in the literature on the broad effects of mixture types on simulation results in a level set context.

2.5 Interface motion

When a physical interface needs to have topology changes because of fluid structure interaction or surface tension for instance, the level set model can follow these changes by a transport step. The idea is to advect the signed distance function, its zero

isovalue representing the interface and all other distant isovales, with the velocity field as input. The motion of the interface is thus expressed by:

$$\frac{d\alpha}{dt} = \frac{\partial\alpha}{\partial t} + \vec{v} \cdot \vec{\nabla}\alpha = 0 \quad (2.58)$$

2.5.1 Level set transport

The finite element method gives the fully discretised weak form of eq. (2.58) by using a convenient set of test functions α^* belonging the Hilbertian *Sobolev* space:

$$\int_{\Omega} \alpha^* \frac{\partial\alpha}{\partial t} d\Omega + \int_{\Omega} \alpha^* \vec{v} \cdot \vec{\nabla}\alpha d\Omega = 0 \quad \forall \alpha^* \in \mathcal{H}^1(\Omega) \quad (2.59)$$

The spatial discretisation of α assigns, for each of the total N nodes of a simplex, the following values:

$$\alpha = \sum_N P_j \alpha_j \quad (2.60)$$

Furthermore, with the standard Galerkin method, we replace test functions by the interpolation functions P_j , then we apply a temporal discretisation for the main unknowns by a forward (implicit) finite difference in time. Consequently, eq. (2.59) can be recast as follows:

$$i, j : 1 \rightarrow \text{Nnodes}$$

$$\frac{1}{\Delta t} (\alpha_j^t - \alpha_j^{t-\Delta t}) \int_{\Omega} P_i P_j d\Omega + \alpha_j^t \int_{\Omega} \vec{v}^t \cdot \vec{\nabla} P_j d\Omega = 0 \quad (2.61a)$$

$$\left[\frac{1}{\Delta t} \int_{\Omega} P_i P_j d\Omega + \int_{\Omega} \vec{v}^t \cdot \vec{\nabla} P_j d\Omega \right] \alpha_j^t = \frac{1}{\Delta t} \int_{\Omega} \alpha^{t-\Delta t} P_i d\Omega \quad (2.61b)$$

$$[\mathcal{M}_{ij} + \mathcal{A}_{ij}] \alpha_j^t = \mathcal{F}_i \quad (2.61c)$$

where \mathcal{M}_{ij} and \mathcal{A}_{ij} are respectively the mass (or capacity) matrix and advection matrix, both written within a local finite element, whereas \mathcal{F}_i is a local vector of known quantities from the previous time step. The solution of the linear system in eq. (2.61c) is the transported distance function.

When the convection regime becomes more dominant diffusion (for high Reynolds number), the standard Galerkin method may lead to instabilities in the solution. In this case, stabilisation is crucial to avoid these oscillations, unless very fine remeshing is done "such that convection no longer dominates on an element level", as stated by [Brooks et al. \[1982\]](#). The authors give a brief explanation of how numerically a convection-dominated equation can lead to oscillatory solutions with the standard Galerkin approximation. They proposed a stabilisation scheme, the Streamline Up-

wind Petrov-Galerkin, better known as SUPG, to stabilise advection dominated Navier-Stokes equations. However, their technique applies to any convection-diffusion equation. The SUPG method consists of modifying the test functions (like a classical Petrov-Galerkin method) by adding artificial diffusion in the flow direction. The modified test function writes:

$$\alpha_{SUPG}^* = \alpha^* + \underbrace{C_{SUPG}^E \left(\vec{v}_{\text{transport}} \cdot \vec{\nabla} \alpha^* \right)}_{\text{Upwind contribution}} \quad (2.62)$$

where the upwind contribution for each finite element E depends on a stabilisation parameter C_{SUPG}^E that is expressed as follows:

$$C_{SUPG}^E = \frac{h^E}{v_{\text{flow}}^E} \quad (2.63)$$

Equation (2.63) shows that the SUPG parameter represents a time constant relative to an element mesh size, h^E , and an average velocity that should represent the magnitude in the flow direction. In the present work, all convection-diffusion equations are stabilised with the SUPG method, namely the conservation of mass, energy, momentum and chemical species as well as the level set transport.

2.5.2 Level set regularisation

Upon transport the distance function field, a crucial property of the level set may be partially or totally lost over the domain, which is:

$$\begin{cases} \|\vec{\nabla} \alpha\| = 1 \\ \alpha(x, t) = 0 & \text{if } x \in \Gamma(t) \end{cases} \quad (2.64)$$

The closer this L^2 -norm to one, the more regular the level set. An irregular distance function induces cumulative numerical errors while transporting distance values far from the interface, resulting in wrong distance information, and loss of properties that make up a "distance function". To show one the benefit of level set regularisation, [Basset \[2006\]](#) states after showing several tests of distance function transport, that regularised distance functions transported with a standard Galerkin method (i.e. without any stabilisation) show better "quality" globally in the domain, compared to initially non-regularised ones. When the transport equation in [eq. \(2.58\)](#) is discretised in time then solved, a *regularisation* (also known as *reinitialisation*) is necessary to conserve as much as possible the property in [eq. \(2.64\)](#).

[Figure 2.5](#) shows the need of regularisation in two different simulations of the same phenomenon: rising air bubble inside water. The importance of this well studied case

[Sussman et al. 1994; Hysing et al. 2009] is that the interface between two fluids is highly deformable as the bubble rises because of buoyancy, and therefore the task of tracking the dynamic interface while maintaining an accurate distance function is a considerable numerical task. In the first simulation, the distance contours are squeezed against the zero-distance contour marked by the thick black line. A closer look to the interface reveals undesired distortions, with a "wavy" shape at some points. This effect is evidently an artefact of a level set transport lacking subsequent reinitialisation, inasmuch as the surface tension tends to minimise the total surface area and make it as smooth as possible. Nevertheless, the second simulation unveils much better results, especially how the interface shows no sign of destabilisation. We also note the regular spacing between contours, which is a consequence of conserving the property defined in eq. (2.64). This improvement is attributed to the regularization done at each time step after the transport. In the forthcoming sections, we present three regularisation methods, then show their strong and weak points.

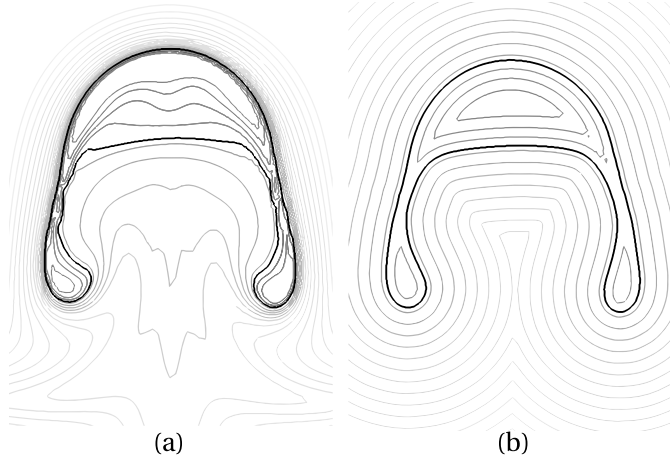


Fig. 2.5 – Schematic of the influence of level set regularisation on the distance function at the same time frame: a) without any regularisation step, the isovalue contours are distorted in the wake of the rising air bubble while being squeezed ahead of it, b) in contrast to regularising the distance function, where the contours maintain their spacing and geometric properties with respect to the tracked interface.

Classic Hamilton-Jacobi reinitialisation

In order to repair a distance function impaired by convective transport, Sussman et al. [1994] proposed solving a classic *Hamilton-Jacobi* equation, given in its most general form:

$$\frac{\partial \alpha}{\partial t} + \mathbb{H}(\alpha, x, t) = 0 \quad x \in \Omega, t > 0 \quad (2.65)$$

where $\alpha(x, t = 0) = \alpha_0$ is the initial value of the distance function. The term \mathbb{H} is known as the *Hamiltonian*. When the sign of the level set and its metric property ($\|\vec{\nabla}\alpha\| = 1$) are considered, eq. (2.65) reduces to:

$$\frac{\partial \alpha}{\partial t} + S(\alpha) (\|\vec{\nabla}\alpha\| - 1) = 0 \quad (2.66)$$

where $S(\alpha)$ is a step function giving the sign of the level set as follows:

$$S(\alpha) = \frac{\alpha}{|\alpha|} = \begin{cases} -1 & \text{if } \alpha < 0 \\ 0 & \text{if } \alpha = 0 \\ +1 & \text{if } \alpha > 0 \end{cases} \quad (2.67)$$

The sign function defined in eq. (2.67) is often smoothed to avoid numerical problems, as proposed for instance by [Sussman et al. \[1994\]](#):

$$S(\alpha) = S_\varepsilon(\alpha) = \frac{\alpha}{\sqrt{\alpha^2 + \varepsilon^2}} \quad (2.68)$$

where ε is a smoothing parameter that depends on the mesh size around the interface. However, one should be aware that within the smoothing thickness, the regularised function may suffer from local oscillations because of the reciprocal reinitialisation taking place at each side of the level set. [Peng et al. \[1999\]](#) states that this problem is more likely to happen if the initial level set shows very weak or very steep gradients, and therefore is not regular enough. The authors eventually propose a new sign function which would reinitialise the distance function, as close as possible to the interface without modifying the latter, as follows:

$$S(\alpha) = S_\varepsilon(\alpha) = \frac{\alpha}{\sqrt{\alpha^2 + \|\vec{\nabla}\alpha\|^2 \varepsilon^2}} \quad (2.69)$$

Convective reinitialization

A recent work by [Ville et al. \[2011\]](#) introduced another concept for reinitialisation called the *convective reinitialisation*. The idea lies in combining both level set advection and regularisation in a single equation, saving resolution time. The key components of their method starts by defining a pseudo time step, $\Delta\tau$, that is linked to the main time variable through a numerical parameter λ_τ , as follows:

$$\lambda_\tau = \frac{\partial \tau}{\partial t} \quad (2.70)$$

The order of magnitude of λ_τ , which can be seen as a relaxation parameter [see [Vigneaux 2007](#), p. 89], is close to the ratio $h/\Delta t$. Then, the classic Hamilton-Jacobi

eq. (2.65) is combined into the convection step by writing:

$$\frac{\partial \alpha}{\partial t} + (\vec{v} + \lambda_\tau \vec{U}) \cdot \vec{\nabla} \alpha = \lambda_\tau S(\alpha) \quad (2.71)$$

where \vec{U} is a velocity vector in the normal direction to the interface, defined by $\vec{U} = S(\alpha) \vec{n}$, the normal vector \vec{n} being previously defined in eq. (2.51). The obvious shortcoming of convective reinitialisation is that it depends on a numerical parameter λ_τ . Another limitation of the method is the use of a sinusoidal filter to modify the distance function by truncating its values beyond a thickness threshold, which is also another parameter to calibrate the resolution. The drawback of truncating the level set is the loss of information far from the interface and the inability to fully reconstruct the distance function. If we denote this threshold by E and the modified level set by $\tilde{\alpha}$ inside the thickness, then eq. (2.71) is recast as:

$$\frac{\partial \alpha}{\partial t} + (\vec{v} + \lambda_\tau \vec{U}) \cdot \vec{\nabla} \alpha = \lambda_\tau S(\alpha) \sqrt{1 - \left(\frac{\pi}{2E} \tilde{\alpha}\right)^2} \quad (2.72)$$

Equation (2.72) describes the transport and partial reconstruction of the distance function α , knowing its value $\tilde{\alpha}$ inside the thickness E .

Geometric reinitialization

This category of methods go from the level set's basic geometric principle to construct a distance function, instead of solving a partial differential system of equations as in the classic Hamilton-Jacobi reinitialisation. A widely known instance of this category is the *fast marching method* developed by [Sethian \[1996\]](#) and influenced by the [Dijkstra \[1959\]](#)'s method to compute the shortest path in a network of nodes. The method aims to solve the eikonal equation in eq. (2.64) to propagate the distance function in a single direction by *upwinding*, i.e. going from low to high values of the distance function, while preserving a unitary distance gradient.

Direct reinitialisation is another interesting method in the geometric reinitialise category. However, it has not gained noticeable attention in the literature given the terrible cost in terms of computation time and efficiency if not optimised. The main idea is very simple: reconstruct the distance function over Ω or a subset of Ω , by computing the minimum distance between each mesh node and the interface. It means that, for any point $\vec{x} \in \Omega$, the following constraint should be satisfied [Osher et al. \[2003\]](#):

$$d_\Gamma(\vec{x}) = \min \|\vec{x} - \vec{x}_\Gamma\| \quad \forall \vec{x}_\Gamma \in \partial\Omega = \Gamma, \quad (2.73)$$

A efficient and optimised implementation of this method is done by [Shakoor et al. \[2015\]](#) making use of *k-d* trees to limit the search operations of elements and the subsequent distance evaluations in each of these elements. Moreover, the authors

Chapter 2. Modelling Review

give a comparison of the previously stated methods on 2D and 3D cases, showing the great performance of direction reinitialisation when used with k-d trees algorithm, hence we use it in the present work.

To do ?

Interface Remeshing: Importance when using a static level set and more importantly when LS is transported, influence of mixing area *thickness* and *resolution* (i.e. nb of nodes with the area), Isotropic or anisotropic ? the first is more important to composition calculation while the second is more relevant if we mean do thermohydraulics without macrosegregation

Chapter 5

Macrosegregation with solidification shrinkage

Contents

5.1 Solidification shrinkage	90
5.2 Multidomain formalism	90
5.2.1 Assumptions	92
5.2.2 Mass balance	93
5.3 FE model: Metal	93
5.3.1 Mass and momentum conservation	93
5.3.2 Energy conservation	95
5.3.3 Species conservation	97
5.4 FE model: Air	99
5.4.1 Mass and momentum conservation	100
5.4.2 Energy conservation	100
5.4.3 Species conservation	100
5.5 FE monolithic model	100
5.5.1 Permeability mixing	100
5.5.2 Model equations	101
5.5.3 Interface treatment	101
5.6 Shrinkage without macrosegregation	103
5.6.1 Al-7wt% Si	104
5.6.2 Pb-3wt% Sn	104
5.7 Shrinkage with macrosegregation	104
5.7.1 Al-7wt% Si	104
5.7.2 Pb-3wt% Sn	104

5.1 Solidification shrinkage

Solidification shrinkage is, by definition, the effect of relative density change between the liquid and solid phases. In general, it results in a progressive volume change during solidification, until the phase change has finished. The four stages in [figs. 5.1a](#) to [5.1d](#) depict the volume change with respect to solidification time. First, at the level of the first solid crust, near the local solidus temperature, the solid forms with a density greater than the liquid's. The subsequent volume decrease creates voids with a negative pressure, forcing the fluid to be sucked in the direction of the volume change (cf. [fig. 5.1b](#)). As a direct result of the inward feeding flow, the ingot surface tends to gradually deform in the feeding direction, forming the so-called *shrinkage pipe*. Since the mass of the alloy and its chemical species is conserved, a density difference between the phases ($\rho^l < \rho^s \implies \frac{\rho^l}{\rho^s} < 1$) eventually leads to a different overall volume ($V^s < V^l$) once solidification is complete, as confirm the following equations:

$$\rho^l V^l = \rho^s V^s \quad (5.1a)$$

$$V^s = \frac{\rho^l}{\rho^s} V^l \quad (5.1b)$$

Solidification shrinkage is not the only factor responsible for volume decrease. Thermal shrinkage in both solid and liquid phases, as well as solutal shrinkage in the liquid phase are also common causes in a casting process. However, thermal shrinkage is very important to apprehend as temperature decrease in steel casting usually exceeds a 1000 °C, causing substantial density variations.

5.2 Multidomain formalism

In the previous chapters, we considered in our simulations the metal as a saturated mixture of solid and liquid during solidification. It means that no gas phase may appear during the process, and this this chapter. The reason is we chose to describe our model in Eulerian description, for which we have considered a fixed grid to discretise the averaged conservation equations governing the phase change between the liquid and solid phases. Furthermore, with the introduction of shrinkage, an increase in global density means that a gas phase should enter the domain to replace the shrunk volume. At this point, several interfaces may be distinguished: liquid-solid (*l-s*), liquid-air (*l-a*) and solid-air (*s-a*), where we defined 2 phases (*l* and *s*) belonging to the "Metal" domain denoted *M*, while the "Air" domain, denoted *A*, is made up of a unique phase, (*a*), with the same name. As a standard for this formalism, we consider that uppercase letters are used for domains, while lowercase letters are used for phases.

The main idea behind the multidomain formalism, is to go from the classic conser-

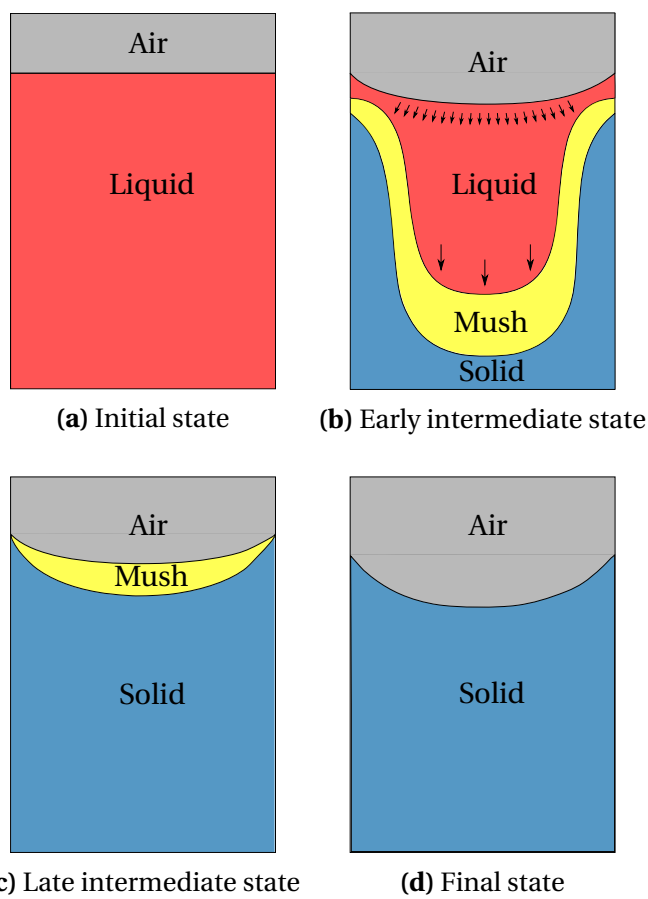


Fig. 5.1 – Schematic of the main cooling stages of an ingot against side and bottom mould walls (not shown)

vations equations introduced by volume averaging in chapter 2, in the context of a solidifying two-phase system to generalise it and take into account a third gas phase that belongs to a new domain, while keeping a physical integrity with the former monodomain model. Then, one is free to choose a suitable numerical method to track the interfaces between the several phases. In our applications, we are particularly interested in keeping an indirect representation of the $l-s$ interface using the volume averaging theory, while employing a different method to track the $l-a$ and $s-a$ interfaces with the level set method. This allows switching to the latter method in a justified and physically representative manner.

In this context, each domain can be seen as a material having a physical interface with the other domains. As a consequence of our interpretation, the gas phase should not exist in the metal, which may naturally occur if the thermodynamic conditions are in favour of nucleating and growing a new phase, or in the case of a gas that was trapped inside mould grooves.

5.2.1 Assumptions

Each phase in the system has its own velocity, \vec{v}^l , \vec{v}^s and \vec{v}^a , while the respective interfaces $l-s$, $l-a$ and $s-a$ have different and independent velocities, represented by \vec{v}^{l-s} , \vec{v}^{l-a} and \vec{v}^{s-a} . Note that the solid-liquid interface velocity was denoted \vec{v}^* in the previous chapters as no more than two phases were considered. The first major assumption is that the solid phase, once formed from the liquid, is fixed and rigid. It means that no subsequent deformation may occur and therefore \vec{v}^{s-a} reduces to vector zero. Moreover, we use the already introduced volume averaging principles to write locally for any quantity ψ :

$$\langle \psi \rangle = \langle \psi^l \rangle + \langle \psi^s \rangle + \langle \psi^a \rangle \quad (5.2a)$$

$$= g^l \psi^l + g^s \psi^s + g^a \psi^a \quad (5.2b)$$

where volume fractions, g^ϕ , for each phase ϕ were used. [Rappaz et al. \[2003\]](#) define the volume fraction by writing a general expression inside the representative volume V_E :

$$g^\phi = \frac{1}{V_E} \int_{V_E} \chi^\phi(x, t) d\Omega \quad (5.3)$$

where the integrated quantity is an indicator (or presence) function relative to phase ϕ , which defines the volume of this phase in the system, Ω^ϕ , as follows:

$$\chi^\phi(x, t) = \begin{cases} 1 & \text{if } x \in \Omega^\phi \\ 0 & \text{otherwise} \end{cases} \quad (5.4)$$

Any phenomenon that may displace an interface, whether by phase change or a phase motion, is mathematically translated by variations of the presence function, i.e. spatial and temporal derivatives of the phase fraction. For a system consisting of two phases, solid and liquid, these variations are given for instance for the liquid by:

$$\frac{\partial \chi^l(x, t)}{\partial t} = \vec{v}^{l-s} \cdot \vec{n}^{l-s} \delta(x - x^{l-s}) = \vec{v}_n^{l-s} \delta(x - x^{l-s}) \quad (5.5)$$

$$\vec{\nabla} \chi^l(x, t) = -\vec{n}^{l-s} \delta(x - x^{l-s}) \quad (5.6)$$

5.2.2 Mass balance

In a real multiphase system containing 3, each phase has its own velocity, \vec{v}^ϕ , which is independent of the interface velocity.

5.3 FE model: Metal

In this section, we start from a the monodomain finite element model presented in [section 2.1.1](#) relevant to metal only, then present the essential assumptions and formulations that allow predicting solidification shrinkage in a Eulerian context.

5.3.1 Mass and momentum conservation

Assumptions

- Two phases are considered, liquid l and solid s : $g^l + g^s = 1$
- The phase densities are constant but not equal: $\rho^l = cst_1$ and $\rho^s = cst_2$. Thermal and solutal expansion/contraction is neglected
- The solid phase is assumed static: $\vec{v}^s = \vec{0}$, which yields the following consequences:

1. $\langle \vec{v} \rangle = g^l \vec{v}^l + g^s \vec{v}^s = g^l \vec{v}^l$
2. $\langle \rho \vec{v} \rangle = g^l \rho^l \vec{v}^l + g^s \rho^s \vec{v}^s = g^l \rho^l \vec{v}^l$
3. $\vec{\nabla} \rho^l = \vec{\nabla} \rho^s = \vec{0}$

Formulation

The mass balance equation averaged over the two phases, is expanded taking into account the aforementioned assumptions.

$$\frac{\partial \langle \rho \rangle}{\partial t} + \nabla \cdot \langle \rho \vec{v} \rangle = 0 \quad (5.7a)$$

$$\frac{\partial}{\partial t} \left(g^l \rho^l + g^s \rho^s \right) + \nabla \cdot \left(g^l \rho^l \vec{v}^l \right) = 0 \quad (5.7b)$$

$$g^l \frac{\partial \rho^l}{\partial t} + \rho^l \frac{\partial g^l}{\partial t} + g^s \frac{\partial \rho^s}{\partial t} + \rho^s \frac{\partial g^s}{\partial t} + \rho^l \nabla \cdot \left(g^l \vec{v}^l \right) + g^l \vec{v}^l \cdot \vec{\nabla} \rho^l = 0 \quad (5.7c)$$

$$\left(\rho^l - \rho^s \right) \frac{\partial g^l}{\partial t} + \rho^l \nabla \cdot \left(g^l \vec{v}^l \right) = 0 \quad (5.7d)$$

$$\nabla \cdot \left(g^l \vec{v}^l \right) = \nabla \cdot \langle \vec{v}^l \rangle = \frac{\rho^l - \rho^s}{\rho^l} \frac{\partial g^s}{\partial t}$$

(5.8)

With the assumptions of static solid phase and constant unequal phase densities, the average mass balance states that the divergence of the liquid velocity is proportional to the solidification rate, by a factor of density change, which results in a relative volume change. [Equation \(5.8\)](#) explains the flow due to shrinkage. In metallic alloys, the solid density is usually greater than the liquid density, therefore the first term in the RHS is negative. As for the second term, if we neglect remelting, then it'll be positive in the solidifying areas of the alloy. A negative divergence term in these areas, means that a liquid feeding is necessary to compensate for the density difference, hence acting as a flow driving force in the melt. In the case of constant densities, we can easily deduce that the divergence term is null, and therefore no flow is induced by solidification. Furthermore, additional terms should appear in the other conservation equations, balancing the volume change in the heat and species transport. When the metal's density was considered constant during solidification, the assumption of an incompressible system made it possible to use the Boussinesq approximation. However, in the case of solidification shrinkage, the average density $\langle \rho \rangle = g^s \rho^s + g^l \rho^l$ varies, since ρ^s and ρ^l are not equal. Naturally, these phase densities would depend on temperature and possibly on the phase composition. Therefore, the incrompressibility condition may not be true. In such case, the earlier given system [eq. \(2.41\)](#) is reformulated without

any reference value for density:

$$\begin{cases} \rho^l \left(\frac{\partial \langle \vec{v}^l \rangle}{\partial t} + \frac{1}{g^l} \vec{\nabla} \cdot (\langle \vec{v}^l \rangle \times \langle \vec{v}^l \rangle) \right) = \\ - g^l \vec{\nabla} p^l - 2\mu^l \vec{\nabla} \cdot (\vec{\nabla} \langle \vec{v}^l \rangle + \vec{\nabla}^t \langle \vec{v}^l \rangle) - g^l \mu^l \mathbb{K}^{-1} \langle \vec{v}^l \rangle + g^l \rho^l \vec{g} \\ \nabla \cdot \langle \vec{v}^l \rangle = \frac{\rho^l - \rho^s}{\rho^l} \frac{\partial g^s}{\partial t} \end{cases} \quad (5.9)$$

5.3.2 Energy conservation

We have seen the averaged energy conservation equation in the case of two phases: a solid phase and an incompressible liquid phase. However, with the incorporation of the shrinkage effect, new terms should appear in the advective-diffusive heat transfer equation.

Assumptions

- The thermal conductivity is constant for both phases: $\langle \kappa \rangle = \langle \kappa^s \rangle = \langle \kappa^l \rangle = \kappa$
- Consequence of the static solid phase: $\langle \rho h \vec{v} \rangle = g^l \rho^l h^l \vec{v}^l + \cancel{g^s \rho^s h^s \vec{v}^s} = g^l \rho^l h^l \vec{v}^l$
- The system's enthalpy may thermodynamically evolve with pressure, knowing that $h = e + \frac{p}{\rho}$, where e is the internal energy and p is the pressure. It infers that the heat transport equation may contain a contribution attributed to volume compression/expansion:

$$\frac{\partial p}{\partial t} + \nabla \cdot (p \vec{v}) = \frac{\partial p}{\partial t} + p \nabla \cdot \vec{v} + \vec{v} \cdot \vec{\nabla} p \quad (5.10)$$

In the literature, this contribution has been always neglected, even when accounting for solidification shrinkage, owing to the small variations of pressure.

- The heat generated by mechanical deformation, $\mathbb{S} : \dot{\varepsilon}$, is neglected

Formulation

The unknowns in the energy conservation are the average volumetric enthalpy $\langle \rho h \rangle$ and temperature T . The energy conservation equation writes:

$$\frac{\partial \langle \rho h \rangle}{\partial t} + \nabla \cdot \langle \rho h \vec{v} \rangle = \nabla \cdot (\langle \kappa \vec{\nabla} T \rangle) \quad (5.11a)$$

$$\frac{\partial \langle \rho h \rangle}{\partial t} + \nabla \cdot (g^l \rho^l h^l \vec{v}^l) = \nabla \cdot (\kappa \vec{\nabla} T) \quad (5.11b)$$

$$\frac{\partial \langle \rho h \rangle}{\partial t} + \rho^l h^l \nabla \cdot \langle \vec{v}^l \rangle + \langle \vec{v}^l \rangle \cdot \vec{\nabla} (\rho^l h^l) = \nabla \cdot (\kappa \vec{\nabla} T) \quad (5.11c)$$

$$\frac{\partial \langle \rho h \rangle}{\partial t} + \cancel{\rho^l h^l} \frac{\rho^l - \rho^s}{\cancel{\rho^l}} \frac{\partial g^s}{\partial t} + \langle \vec{v}^l \rangle \cdot \vec{\nabla} (\rho^l h^l) = \nabla \cdot (\kappa \vec{\nabla} T) \quad (5.11d)$$

$$\frac{\partial \langle \rho h \rangle}{\partial t} + (\rho^l - \rho^s) h^l \frac{\partial g^s}{\partial t} + \langle \vec{v}^l \rangle \cdot \vec{\nabla} (\rho^l h^l) = \nabla \cdot (\kappa \vec{\nabla} T) \quad (5.11e)$$

$$\frac{\partial \langle \rho h \rangle}{\partial t} + \rho^l \langle \vec{v}^l \rangle \cdot \vec{\nabla} h^l = \nabla \cdot (\kappa \vec{\nabla} T) + (\rho^s - \rho^l) h^l \frac{\partial g^s}{\partial t} \quad (5.12)$$

In order to keep things simple, the term "enthalpy" will refer henceforth to "volume enthalpy", otherwise, we will explicitly use the term "mass enthalpy". It is important to understand the meaning of the terms in equation (5.12). The first term in the left-hand side is the temporal change in the system's average enthalpy, i.e. a temporal change in the volume enthalpy of any of the phases in the course of solidification. The second LHS term is a dot product between the superficial liquid velocity and the gradient of the liquid's enthalpy. Since phase densities are constant in our case, the gradient term reduces to the liquid's mass enthalpy. If we consider a representative volume element (RVE) in the liquid phase, far from the mushy zone, we can stipulate:

$$\vec{\nabla} h^l = C_p^l \vec{\nabla} T \quad (5.13)$$

assuming that the phase mass specific heat, C_p^l , is constant. Therefore, the liquid enthalpy is advected in the case where the velocity vector is not orthogonal to the temperature gradient. The advection reaches its maximum when the two vectors have the same direction. Consider, for instance, a filled ingot with a cooling flux applied to its bottom surface. If the density variation with temperature were to be neglected, then the sole mechanical driving force in the melt is the density jump at the solid-liquid interface ahead of the mushy zone. The temperature gradient in such a case is vertical upward, while the velocity vector is in the opposite direction. The advective term writes:

$$\rho^l \langle \vec{v}^l \rangle \cdot \vec{\nabla} h^l = -\rho^l C_p^l \|\langle \vec{v}^l \rangle\| \|\vec{\nabla} T\| \quad (5.14)$$

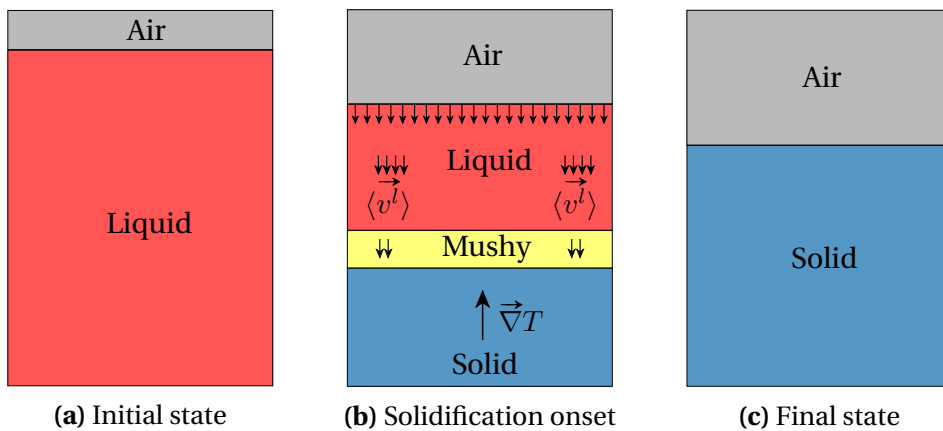


Fig. 5.2 – Effect of one-dimensional shrinkage flow on a solidifying ingot

We see that the second LHS term in equation (5.12) acts as a heat source at the interface between the the phases, in this particular solidification scenario. Another heat power (of unit Wm^{-3}) adds to the system in the mushy zone, that is the second term in the RHS of the same equation. This term is proportional to the solidification rate. Finally, the first RHS term accounts for thermal diffusion within the phases.

It should be emphasized that the assumption of a constant specific heat in the liquid in equation (5.13) applies when no macrosegregation occurs. Nonetheless, when the latter is considered, the phases specific and latent heats become highly dependent on the local average composition. It then advisable to use the thermodynamic tabulation approach, where the enthalpies are directly tabulated as functions of temperature and intrinsic phase compositions.

5.3.3 Species conservation

The last conservation principle is applied to the chemical species or solutes. This principle allows predicting macrosegregation when applied to a solidification system, along with the mass, momentum and energy balances. However, the conservation equation should be reformulated in the case of a melt flow driven by shrinkage.

Assumptions

- The alloy is binary, i.e. it is composed from one solute, and hence the notation of the average composition without a solute index: $\langle w \rangle$ for the mass composition and $\langle \rho w \rangle$ for the volume composition
- The solid fration is determined assuming complete mixing in both phases, hence the lever rule is applied. The solidification path in the current approach is tabulated using thermodynamic data at equilibrium

Chapter 5. Macrosegregation with solidification shrinkage

- The macroscopic solute diffusion coefficient D^s in the solid phase is neglected in the mass diffusive flux term.
- The solid phase is fixed and rigid, therefore $\langle \rho w \vec{v} \rangle = g^l \rho^l \langle w \rangle^l \vec{v}^l + g^s \rho^s \langle w \rangle^s \vec{v}^s = g^l \rho^l \langle w \rangle^l \vec{v}^l$

Formulation

The species conservation is pretty similar the energy conservation formulated in the previous section. For a binary alloy, we write:

$$\frac{\partial \langle \rho w \rangle}{\partial t} + \nabla \cdot \langle \rho w \vec{v} \rangle - \nabla \cdot \left(\langle D^l \rangle \vec{\nabla} (\rho^l \langle w \rangle^l) \right) = 0 \quad (5.15a)$$

$$\langle \rho \rangle \frac{\partial \langle w \rangle}{\partial t} + \langle w \rangle \frac{\partial \langle \rho \rangle}{\partial t} + \nabla \cdot \left(g^l \rho^l \langle w \rangle^l \vec{v}^l \right) - \nabla \cdot \left(g^l D^l \vec{\nabla} (\rho^l \langle w \rangle^l) \right) = 0 \quad (5.15b)$$

$$\begin{aligned} & \langle \rho \rangle \frac{\partial \langle w \rangle}{\partial t} + \langle w \rangle \frac{\partial \langle \rho \rangle}{\partial t} + \left(\rho^l \langle w \rangle^l \right) \nabla \cdot \langle \vec{v}^l \rangle + \langle \vec{v}^l \rangle \cdot \vec{\nabla} (\rho^l \langle w \rangle^l) \\ & - \nabla \cdot \left(g^l D^l \vec{\nabla} (\rho^l \langle w \rangle^l) \right) = 0 \end{aligned} \quad (5.15c)$$

The mass balance gives the following relations:

$$\frac{\partial \langle \rho \rangle}{\partial t} + \nabla \cdot \langle \rho \vec{v} \rangle = 0 \quad (5.16a)$$

$$\frac{\partial \langle \rho \rangle}{\partial t} + \nabla \cdot \left(g^l \rho^l \vec{v}^l \right) = 0 \quad (\rho^l \text{ is constant}) \quad (5.16b)$$

$$\nabla \cdot \langle \vec{v}^l \rangle = -\frac{1}{\rho^l} \frac{\partial \langle \rho \rangle}{\partial t} \quad (5.16c)$$

If we use the result of eq. (5.16c) in eq. (5.15c), then we get the following equation:

$$\langle \rho \rangle \frac{\partial \langle w \rangle}{\partial t} + \langle w \rangle \frac{\partial \langle \rho \rangle}{\partial t} = \langle w \rangle^l \frac{\partial \langle \rho \rangle}{\partial t} - \langle \vec{v}^l \rangle \cdot \vec{\nabla} (\rho^l \langle w \rangle^l) + \nabla \cdot \left(g^l D^l \vec{\nabla} (\rho^l \langle w \rangle^l) \right) \quad (5.17)$$

Applying Voller-Prakash [Voller et al. 1989] variable splitting, the system ends up with only one variable, which is the average composition $\langle w \rangle$. The splitting is done as follows:

$$\langle w \rangle^l = \left(\langle w \rangle^l \right)^t + \langle w \rangle - \langle w \rangle^t \quad (5.18)$$

where the superscript t refers to the previous time step. The chemical species conservation writes:

$$\begin{aligned} \langle \rho \rangle \frac{\partial \langle w \rangle}{\partial t} + \cancel{\langle w \rangle} \frac{\partial \langle \rho \rangle}{\partial t} = \\ \cancel{\langle w \rangle} \frac{\partial \langle \rho \rangle}{\partial t} - \rho^l \langle v^l \rangle \cdot \vec{\nabla} \langle w \rangle + \nabla \cdot (g^l \rho^l D^l \nabla \langle w \rangle) \\ + \frac{\partial \langle \rho \rangle}{\partial t} \left[(\langle w \rangle^l)^t - \langle w \rangle^t \right] - \rho^l \langle v^l \rangle \cdot \vec{\nabla} \left(\langle w \rangle^t - (\langle w \rangle^l)^t \right) \end{aligned} \quad (5.19a)$$

$$\begin{aligned} \langle \rho \rangle \frac{\partial \langle w \rangle}{\partial t} + \rho^l \langle v^l \rangle \cdot \vec{\nabla} \langle w \rangle - \nabla \cdot (g^l \rho^l D^l \nabla \langle w \rangle) = \\ - \frac{\partial \langle \rho \rangle}{\partial t} \left[\langle w \rangle^t - (\langle w \rangle^l)^t \right] + \rho^l \langle v^l \rangle \cdot \vec{\nabla} \left(\langle w \rangle^t - (\langle w \rangle^l)^t \right) \\ - \nabla \cdot [g^l \rho^l D^l \vec{\nabla} \left(\langle w \rangle^t - (\langle w \rangle^l)^t \right)] \end{aligned} \quad (5.19b)$$

$$\begin{aligned} \langle \rho \rangle \frac{\partial \langle w \rangle}{\partial t} + \rho^l \langle v^l \rangle \cdot \vec{\nabla} \langle w \rangle - \nabla \cdot (g^l \rho^l D^l \nabla \langle w \rangle) = \\ - \frac{\partial \langle \rho \rangle}{\partial t} \left[\langle w \rangle^t - (\langle w \rangle^l)^t \right] \\ + \rho^l \langle v^l \rangle \cdot \vec{\nabla} \left(\langle w \rangle^t - (\langle w \rangle^l)^t \right) - \nabla \cdot [g^l \rho^l D^l \vec{\nabla} \left(\langle w \rangle^t - (\langle w \rangle^l)^t \right)] \end{aligned} \quad (5.20)$$

It is noted that eq. (5.20) is valid only if both densities ρ^l and ρ^s are constant but have different values. Since density changes are incorporated in this equation, inverse segregation following solidification shrinkage is predicted. For the case where macrosegregation is solely due to fluid flow generated by natural or forced convection, i.e. no shrinkage occurs whether due to thermal-solutal contraction or phase change, the overall volume remains constant, hence density is constant. In this situation, $\rho^s = \rho^l = \langle \rho \rangle$ and the term $\partial \langle \rho \rangle / \partial t$ therefore vanishes. After dividing both sides by $\langle \rho \rangle = \rho^l$, eq. (5.20) reduces to:

$$\begin{aligned} \frac{\partial \langle w \rangle}{\partial t} + \langle v^l \rangle \cdot \vec{\nabla} \langle w \rangle - \nabla \cdot (g^l D^l \nabla \langle w \rangle) \\ = \langle v^l \rangle \cdot \vec{\nabla} \left(\langle w \rangle^t - (\langle w \rangle^l)^t \right) - \nabla \cdot [g^l D^l \vec{\nabla} \left(\langle w \rangle^t - (\langle w \rangle^l)^t \right)] \end{aligned} \quad (5.21)$$

5.4 FE model: Air

Conservation equations for the air are close to those derived for the metal as a fluid, with the exception of some points:

- air is a fluid that will not undergo any phase change, hence constant heat diffusivity;
- species conservation is irrelevant in the air as it is considered a pure material;
- unlike metal, air is considered incompressible at any time.

5.4.1 Mass and momentum conservation

5.4.2 Energy conservation

5.4.3 Species conservation

The composition of alloying elements is crucial quantity to predict in this work. Nevertheless, such prediction is only relevant in the metallic alloy, even if the air is also made up of other chemical species (nitrogen, oxygen ...). For this obvious reason, the species conservation equation should not be solved in the air, but that of course is contradictory to the monolithic resolution. The consequence is that we should compute the conservation of chemical species in the air and the metal, but limit as much as possible the influence of the former, in a way to prevent a "numerical" solute exchange between these domains. To do so, the computed air velocity will not be used here for advection, but rather use a zero-velocity vector instead. As diffusion is also another transport mechanism that may alter the conservation principle, a very low macroscopic solute diffusion coefficient can be used, as long as its order of magnitude is at most a thousand times less than that in the melt, $D^A \ll D^l$. The low artificial diffusion in the air may slightly violate the wanted no-exchange condition at the air-liquid interface, but it is known that suppressing the diffusion term in the air would result in a stiff partial differential equation that may be difficult to solve.

$$\frac{\partial}{\partial t} (\rho^A \langle w \rangle^A) + \nabla \cdot (\rho^A \langle w \rangle^A \vec{v}^a) - \nabla \cdot (\rho^A D^A \vec{\nabla} \langle w \rangle^A) = 0 \quad (5.22)$$

$$\boxed{\frac{\partial}{\partial t} (\rho^A \langle w \rangle^A) - \nabla \cdot (\rho^A D^A \vec{\nabla} \langle w \rangle^A) = 0} \quad (5.23)$$

5.5 FE monolithic model

The monolithic model combines all conservations equations in metal and air in a unique set of equations to be solved on a fixed mesh. This can be accomplished by using the Heaviside function (defined in [section 2.4.1](#)) relative to each domain.

5.5.1 Permeability mixing

How to mix liquid fraction, best using harmonic or arithmetic, in order to replicate the effect the of non slip condition at top for example

Put the python plots from the presentations in "TEXUS monolithic"
Put video animations of PSEUDO SMACS 2D without and with LS ???

5.5.2 Model equations

Rewrite air-metal monolithic conservation equations using mixture laws.

5.5.3 Interface treatment

The level set method, like any other interface tracking/capturing method, needs defining a convenient way of coupling the velocity field on the one hand, which is the solution provided by solving momentum conservation equations, with the interface position on the other hand. The question is "how does the velocity field transport the interface?". The answer is potentially one of two possibilities: classical coupling or modified coupling. In the next subsections, we discuss the technical details of each approach and the hurdles that come with it.

Classical coupling

A "classical" coupling comes in the sense of "unmodified" coupling. This approach consists of taking the output of the fluid mechanics solver, then feed it as raw input to level set transport solver. The physical translation would be that the interface motion is dictated by the fluids flow in its vicinity. No treatment whatsoever is done between the two mentioned steps. While conservation principles are best satisfied with this approach, the latter yields some drawbacks, preventing its application in a generic way. For instance, the free liquid surface is not necessarily horizontal at all times and that can lead to the wrong shrinkage profile when solidification is complete.

present the example of unstable interface when the ratio between fluids properties became greater than some value+discussion

Modified coupling

In contrast to a classic coupling, here we attempt to modify the velocity field before feeding to the transport solver. The main motivation for considering this approach is the lack of stability that we observed whenever the mechanical properties of the fluids were different by several orders of magnitude. The algorithm should simultaneously fulfil these requirements:

- support high ratios of fluids density with close viscosities by preserving an non-oscillating interface,
- maintain a horizontal level at the free surface of the melt,
- follow shrinking metal surface profile in solidifying regions,

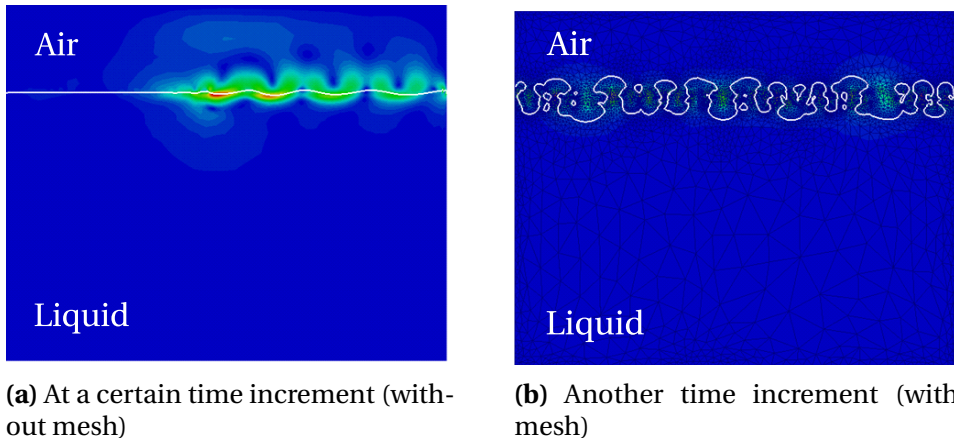


Fig. 5.3 – Interface destabilisation under the effect of high properties ratio across the interface.

- satisfy the mass conservation principle, essentially in the metal.

We want to process the original transport velocity by imposing a uniform motion (speed and direction) at the nodes of the free surface, and at the same time, be able to follow the pipe formation at the surface as a result of solidification shrinkage, as shown in [fig. 5.4](#).

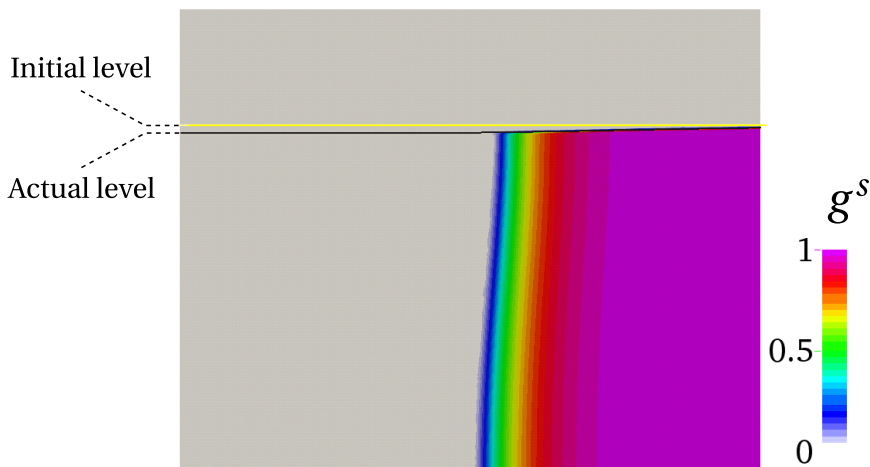


Fig. 5.4 – Snapshot of a solidifying ingot by a cooling flux from the side. The profile of the actual surface changes in solid and mushy regions to adapt the new density while staying perfectly horizontal in the liquid phase.

How to transport level set using velocity from momentum conservation DIRECTLY or AVERAGED PER ELEMENTS, show examples of instability/stability when using false/nominal air properties

Validation of LS transport: perform test case simulation of buoyancy driven air droplet in water by 2005Nagragh that I also have seen in Shyamprasad's masters report). => I didnt notice: what time step δt did they use ?

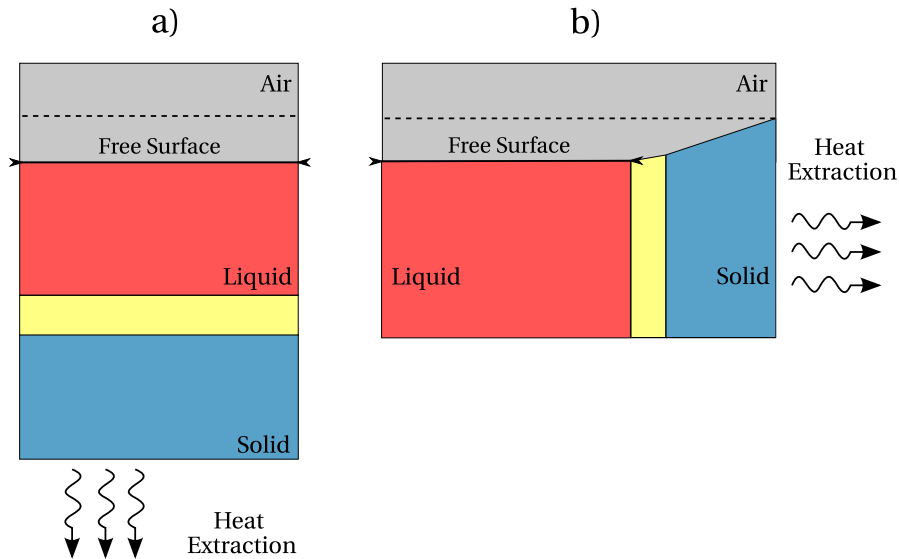


Fig. 5.5 – Treatment of liquid free surface in a) bottom and b) side heat extraction configurations. The dashed line represents the initial level of the free liquid surface.

The general idea is read the velocity around the interface up to a certain thickness, which may be the same thickness as the diffuse interface defined in [section 2.4.1](#), then compute a volumetric average from all the elements in the thickness. This average is then given to the transport solver, which will apply the same magnitude and direction to transport the interface. However, as we only need the transport velocity to be uniform within the "100% liquid" elements, it should not be the case for the other elements that belong either to the mushy zone or the solid region, where shrinkage is taking place. Therefore, depending on the heat extraction configuration, two scenarios are possible. If heat extraction is far from the interface, i.e. there is not direct contact as in [fig. 5.5a](#), the surface area remains unchanged at any time, hence all the elements around the interface are "100% liquid". This happens when a bottom cooling is applied to the ingot. In contrast, if a side cooling is applied as shown in [fig. 5.5b](#), the surface area of the interface will be reduced over time as a consequence of the solid front progression. In this case, the average transport velocity should be computed only from the elements belonging to the free surface. The remaining part of the interface which belongs to partial or full solid regions, is transported with Navier-Stokes output, which should be some orders of magnitude less than the velocity imposed at the free surface, as a result of a decreasing permeability.

5.6 Shrinkage without macrosegregation

Explain how the flow and heat transfer in the air are not important

Give the strong form equations to be solved OR simply refer the previous section where

Chapter 5. Macrosegregation with solidification shrinkage

the model was defined

Initial and boundary conditions for energy and momentum: Initially we have liquid and air at rest.

5.6.1 Al-7wt% Si

Present pseudo 1D case with results + discussion

5.6.2 Pb-3wt% Sn

Present 2D and 3D case with results + discussion

5.7 Shrinkage with macrosegregation

Explain how the flow and heat transfer in the air are not important

Give the strong form equations to be solved OR simply refer the previous section where the model was defined

Initial and boundary conditions for energy and momentum: Initially we have liquid and air at rest.

5.7.1 Al-7wt% Si

Present pseudo 1D case with results + discussion

5.7.2 Pb-3wt% Sn

Present 2D and 3D case with results + discussion

Bibliography

[Andersson et al. 2002]

Andersson, J.-O., Helander, T., Höglund, L., Shi, P., and Sundman, B. (2002). “Thermo-Calc & DICTRA, computational tools for materials science”. *Calphad*, 26 (2), pp. 273–312. URL: <http://www.sciencedirect.com/science/article/pii/S0364591602000378>.

[Arnold et al. 1984]

Arnold, D. N., Brezzi, F., and Fortin, M. (1984). “A stable finite element for the stokes equations”. *CALCOLO*, 21 (4), pp. 337–344. URL: <http://link.springer.com/article/10.1007/BF02576171>.

[Aubertin et al. 2000]

Aubertin, P., Wang, T., Cockcroft, S. L., and Mitchell, A. (2000). “Freckle formation and freckle criterion in superalloy castings”. *Metallurgical and Materials Transactions B*, 31 (4), pp. 801–811. URL: <http://link.springer.com/article/10.1007/s11663-000-0117-9>.

[Aubertin 1998]

Aubertin, P. B. L. (1998). “Determination of the influence of growth front angle on freckle formation in superalloys”. PhD thesis. Vancouver, BC, Canada: University of British Columbia. URL: https://circle.ubc.ca/bitstream/handle/2429/8676/ubc_1998-345084.pdf?sequence=1.

[Basset 2006]

Basset, O. (2006). “Simulation numérique d’écoulements multi-fluides sur grille de calcul”. PhD Thesis. École Nationale Supérieure des Mines de Paris. URL: <https://tel.archives-ouvertes.fr/tel-00376484> (cited on page 32).

[Beckermann 2002]

Beckermann, C. (2002). “Modelling of macrosegregation: applications and future needs”. *International Materials Reviews*, 47 (5), pp. 243–261. URL: <http://www.maneyonline.com/doi/abs/10.1179/095066002225006557> (cited on page 8).

[Beckermann et al. 1999]

Beckermann, C., Diepers, H. J., Steinbach, I., Karma, A., and Tong, X (1999). “Modeling Melt Convection in Phase-Field Simulations of Solidification”. *Journal of Computational Physics*, 154 (2), pp. 468–496. URL: <http://www.sciencedirect.com/science/article/pii/S0021999199963234> (cited on page 27).

Bibliography

[Beckermann et al. 2000]

Beckermann, C., Gu, J. P., and Boettinger, W. J. (2000). "Development of a freckle predictor via rayleigh number method for single-crystal nickel-base superalloy castings". *Metallurgical and Materials Transactions A*, 31 (10), pp. 2545–2557. URL: <http://link.springer.com/article/10.1007/s11661-000-0199-7>.

[Bellet et al. 2009]

Bellet, M. et al. (2009). "Call for contributions to a numerical benchmark problem for 2D columnar solidification of binary alloys". *International Journal of Thermal Sciences*, 48 (11), pp. 2013–2016. URL: <http://www.sciencedirect.com/science/article/pii/S129007290900177X>.

[Boden et al. 2008]

Boden, S., Eckert, S., Willers, B., and Gerbeth, G. (2008). "X-Ray Radioscopic Visualization of the Solutal Convection during Solidification of a Ga-30 Wt Pct In Alloy". *Metallurgical and Materials Transactions A*, 39 (3), pp. 613–623. URL: <http://link.springer.com/article/10.1007/s11661-007-9462-5>.

[Boettinger et al. 2002]

Boettinger, W. J., Warren, J. A., Beckermann, C., and Karma, A. (2002). "Phase-Field Simulation of Solidification1". *Annual Review of Materials Research*, 32 (1), pp. 163–194. URL: <http://dx.doi.org/10.1146/annurev.matsci.32.101901.155803> (cited on page 25).

[Bogno et al. 2013]

Bogno, A., Nguyen-Thi, H., Reinhart, G., Billia, B., and Baruchel, J. (2013). "Growth and interaction of dendritic equiaxed grains: In situ characterization by synchrotron X-ray radiography". *Acta Materialia*, 61 (4), pp. 1303–1315. URL: <http://www.sciencedirect.com/science/article/pii/S1359645412008026> (cited on page 6).

[Brackbill et al. 1992]

Brackbill, J. U., Kothe, D. B., and Zemach, C (1992). "A continuum method for modeling surface tension". *Journal of Computational Physics*, 100 (2), pp. 335–354. URL: <http://www.sciencedirect.com/science/article/pii/002199919290240Y> (cited on page 28).

[Brooks et al. 1982]

Brooks, A. N. and Hughes, T. J. R. (1982). "Streamline upwind/Petrov-Galerkin formulations for convection dominated flows with particular emphasis on the incompressible Navier-Stokes equations". *Computer Methods in Applied Mechanics and Engineering*, 32 (1–3), pp. 199–259. URL: <http://www.sciencedirect.com/science/article/pii/0045782582900718> (cited on page 31).

[Buffet et al. 2010]

Buffet, A. et al. (2010). "Measurement of Solute Profiles by Means of Synchrotron X-Ray Radiography during Directional Solidification of Al-4 wt% Cu Alloys". *Materials Science Forum*, 649, pp. 331–336. URL: <http://www.scientific.net/MSF.649.331> (cited on page 6).

[Carozzani et al. 2012]

Carozzani, T., Digonnet, H., and Gandin, C.-A. (2012). “3D CAFE modeling of grain structures: application to primary dendritic and secondary eutectic solidification”. *Modelling and Simulation in Materials Science and Engineering*, 20 (1), p. 015010. URL: <http://iopscience.iop.org/0965-0393/20/1/015010>.

[Carozzani et al. 2014]

Carozzani, T., Gandin, C.-A., and Digonnet, H. (2014). “Optimized parallel computing for cellular automaton-finite element modeling of solidification grain structures”. *Modelling and Simulation in Materials Science and Engineering*, 22 (1), p. 015012. URL: <http://iopscience.iop.org/0965-0393/22/1/015012>.

[Carozzani 2012]

Carozzani, T. (2012). “Développement d’un modèle 3D Automate Cellulaire-Éléments Finis (CAFE) parallèle pour la prédiction de structures de grains lors de la solidification d’alliages métalliques”. PhD Thesis. Ecole Nationale Supérieure des Mines de Paris. URL: <http://pastel.archives-ouvertes.fr/pastel-00803282> (cited on page 12).

[Carozzani et al. 2013]

Carozzani, T. et al. (2013). “Direct Simulation of a Solidification Benchmark Experiment”. *Metallurgical and Materials Transactions A*, 44 (2), pp. 873–887. URL: <http://link.springer.com/article/10.1007/s11661-012-1465-1>.

[Chen et al. 1997]

Chen, S., Merriman, B., Osher, S., and Smereka, P. (1997). “A Simple Level Set Method for Solving Stefan Problems”. *Journal of Computational Physics*, 135 (1), pp. 8–29. URL: <http://www.sciencedirect.com/science/article/pii/S0021999197957211> (cited on page 25).

[Chen 2014]

Chen, S. (2014). “Three dimensional Cellular Automaton - Finite Element (CAFE) modeling for the grain structures development in Gas Tungsten / Metal Arc Welding processes”. PhD Thesis. Ecole Nationale Supérieure des Mines de Paris. URL: <https://pastel.archives-ouvertes.fr/pastel-01038028> (cited on page 26).

[Choudhary et al. 2007]

Choudhary, S. K. and Ganguly, S. (2007). “Morphology and Segregation in Continuously Cast High Carbon Steel Billets”. *ISIJ International*, 47 (12), pp. 1759–1766 (cited on page 3).

[Clyne et al. 1981]

Clyne, T. W. and Kurz, W. (1981). “Solute redistribution during solidification with rapid solid state diffusion”. *Metallurgical Transactions A*, 12 (6), pp. 965–971. URL: <http://link.springer.com/article/10.1007/BF02643477> (cited on page 17).

[Combeau et al. 1996]

Combeau, H., Drezet, J.-M., Mo, A., and Rappaz, M. (1996). “Modeling of microsegregation in macrosegregation computations”. *Metallurgical and Materials Transactions A*,

Bibliography

27 (8), pp. 2314–2327. URL: <http://link.springer.com/article/10.1007/BF02651886> (cited on page 17).

[Combeau et al. 2009]

Combeau, H., Založník, M., Hans, S., and Richy, P. E. (2009). “Prediction of Macrosegregation in Steel Ingots: Influence of the Motion and the Morphology of Equiaxed Grains”. *Metallurgical and Materials Transactions B*, 40 (3), pp. 289–304. URL: <http://link.springer.com/article/10.1007/s11663-008-9178-y> (cited on page 2).

[Copley et al. 1970]

Copley, S. M., Giamei, A. F., Johnson, S. M., and Hornbecker, M. F. (1970). “The origin of freckles in unidirectionally solidified castings”. *Metallurgical Transactions*, 1 (8), pp. 2193–2204. URL: <http://link.springer.com/article/10.1007/BF02643435>.

[Courtois et al. 2014]

Courtois, M., Carin, M., Masson, P. L., Gaied, S., and Balabane, M. (2014). “A complete model of keyhole and melt pool dynamics to analyze instabilities and collapse during laser welding”. *Journal of Laser Applications*, 26 (4), p. 042001. URL: <http://scitation.aip.org/content/lia/journal/jla/26/4/10.2351/1.4886835> (cited on page 26).

[Dantzig et al. 2009]

Dantzig, J. A. and Rappaz, M. (2009). *Solidification*. EPFL Press (cited on pages 5, 9, 17, 18, 20, 21).

[Darcy 1856]

Darcy, H. (1856). *Les fontaines publiques de la ville de Dijon : exposition et application des principes à suivre et des formules à employer dans les questions de distribution d'eau*. V. Dalmont (Paris). URL: <http://gallica.bnf.fr/ark:/12148/bpt6k624312> (cited on page 6).

[Desbiolles et al. 2003]

Desbiolles, J.-L., Thévoz, P., Rappaz, M., and Stefanescu, D. (2003). “Micro-Macrosegregation Modeling in Casting: A Fully Coupled 3D Model”. TMS Publ., pp. 245–252.

[Desmaison et al. 2014]

Desmaison, O., Bellet, M., and Guillemot, G. (2014). “A level set approach for the simulation of the multipass hybrid laser/GMA welding process”. *Computational Materials Science*, 91, pp. 240–250. URL: <http://www.sciencedirect.com/science/article/pii/S092702561400278X> (cited on page 26).

[Digonnet et al. 2007]

Digonnet, H., Silva, L., and Coupez, T. (2007). “Cimlib: A Fully Parallel Application For Numerical Simulations Based On Components Assembly”. *AIP Conference Proceedings*. Vol. 908. AIP Publishing, pp. 269–274. URL: <http://scitation.aip.org/content/aip/proceeding/aipcp/10.1063/1.2740823> (cited on page 13).

[Dijkstra 1959]

Dijkstra, E. W. (1959). “A note on two problems in connexion with graphs”. *Numerische*

- Mathematik*, 1 (1), pp. 269–271. URL: <http://link.springer.com/article/10.1007/BF01386390> (cited on page 35).
- [DLR 2014]**
DLR (2014). *ElectoMagnetic Levitation*. <http://goo.gl/e5JhiA> (cited on page 12).
- [Doré et al. 2000]**
Doré, X., Combeau, H., and Rappaz, M. (2000). “Modelling of microsegregation in ternary alloys: Application to the solidification of Al–Mg–Si”. *Acta Materialia*, 48 (15), pp. 3951–3962. URL: <http://www.sciencedirect.com/science/article/pii/S1359645400001774>.
- [Du et al. 2007]**
Du, Q., Eskin, D. G., and Katgerman, L. (2007). “Modeling Macrosegregation during Direct-Chill Casting of Multicomponent Aluminum Alloys”. *Metallurgical and Materials Transactions A*, 38 (1), pp. 180–189. URL: <http://link.springer.com/article/10.1007/s11661-006-9042-0>.
- [Du et al. 2001]**
Du, Q., Li, D., Li, Y., Li, R., and Zhang, P. (2001). “Simulating a double casting technique using level set method”. *Computational Materials Science*, 22 (3–4), pp. 200–212. URL: <http://www.sciencedirect.com/science/article/pii/S0927025601001902> (cited on page 26).
- [Easton et al. 2011]**
Easton, M., Davidson, C., and StJohn, D. (2011). “Grain Morphology of As-Cast Wrought Aluminium Alloys”. *Materials Transactions*, 52 (5), pp. 842–847 (cited on page 5).
- [Ettrich et al. 2014]**
Ettrich, J. et al. (2014). “Modelling of transient heat conduction with diffuse interface methods”. *Modelling and Simulation in Materials Science and Engineering*, 22 (8), p. 085006. URL: <http://iopscience.iop.org/0965-0393/22/8/085006> (cited on page 30).
- [Felicelli et al. 1991]**
Felicelli, S. D., Heinrich, J. C., and Poirier, D. R. (1991). “Simulation of freckles during vertical solidification of binary alloys”. *Metallurgical Transactions B*, 22 (6), pp. 847–859. URL: <http://link.springer.com/article/10.1007/BF02651162> (cited on page 6).
- [Felicelli et al. 1998]**
Felicelli, S. D., Poirier, D. R., and Heinrich, J. C. (1998). “Modeling freckle formation in three dimensions during solidification of multicomponent alloys”. *Metallurgical and Materials Transactions B*, 29 (4), pp. 847–855. URL: <http://link.springer.com/article/10.1007/s11663-998-0144-5>.
- [Ferreira et al. 2004]**
Ferreira, I. L., Garcia, A., and Nestler, B. (2004). “On macrosegregation in ternary Al–Cu–Si alloys: numerical and experimental analysis”. *Scripta Materialia*, 50 (4), pp. 407–411. URL: <http://www.sciencedirect.com/science/article/pii/S1359646203007346> (cited on page 7).

Bibliography

[Ferreira et al. 2009]

Ferreira, I., Moutinho, D., Gomes, L., Rocha, O., and Garcia, A. (2009). “Modeling and experimental analysis of macrosegregation during transient solidification of a ternary Al–6wt%Cu–1wt%Si alloy”. *Philosophical Magazine Letters*, 89 (12), pp. 769–777. URL: <http://dx.doi.org/10.1080/09500830903292320> (cited on page 7).

[Flemings 1974]

Flemings, M. C. (1974). “Solidification processing”. *Metallurgical Transactions*, 5 (10), pp. 2121–2134. URL: <http://link.springer.com/article/10.1007/BF02643923> (cited on page 3).

[Flemings et al. 1967]

Flemings, M. C. and Nereo, G. E. (1967). “Macrosegregation: Part I”. *Transactions of the Metallurgical Society of AIME*, 239, pp. 1449–1461 (cited on page 6).

[Flemings et al. 1968a]

Flemings, M. C., Mehrabian, R., and Nereo, G. E. (1968a). “Macrosegregation: Part II”. *Transactions of the Metallurgical Society of AIME*, 242, pp. 41–49 (cited on page 6).

[Flemings et al. 1968b]

Flemings, M. C. and Nereo, G. E. (1968b). “Macrosegregation: Part III”. *Transactions of the Metallurgical Society of AIME*, 242, pp. 50–55 (cited on page 6).

[Gada et al. 2009]

Gada, V. H. and Sharma, A. (2009). “On Derivation and Physical Interpretation of Level Set Method-Based Equations for Two-Phase Flow Simulations”. *Numerical Heat Transfer, Part B: Fundamentals*, 56 (4), pp. 307–322. URL: <http://dx.doi.org/10.1080/10407790903388258> (cited on page 28).

[Gandin 2000]

Gandin, C. A. (2000). “From constrained to unconstrained growth during directional solidification”. *Acta Materialia*, 48 (10), pp. 2483–2501. URL: <http://www.sciencedirect.com/science/article/pii/S1359645400000707>.

[Gandin et al. 2003]

Gandin, C. A., Guillemot, G., Appolaire, B., and Niane, N. T. (2003). “Boundary layer correlation for dendrite tip growth with fluid flow”. *Materials Science and Engineering: A*, 342 (1–2), pp. 44–50. URL: <http://www.sciencedirect.com/science/article/pii/S0921509302002617>.

[Genereux et al. 2000]

Genereux, P. D. and Borg, C. A. (2000). “Characterization of Freckles in a High Strength Wrought Nickel Superalloy”. Warrendale, PA: K.A. Green, M. McLean, S. Olson, J.J. Schirra, TMS (The Minerals, Metals, and Materials Society), pp. 19–27. URL: http://www.tms.org/superalloys/10.7449/2000/Superalloys_2000_19_27.pdf.

[Giamei et al. 1970]

Giamei, A. F. and Kear, B. H. (1970). “On the nature of freckles in nickel base superalloys”.

- Metallurgical Transactions*, 1 (8), pp. 2185–2192. URL: <http://link.springer.com/article/10.1007/BF02643434>.
- [Gibou et al. 2003]**
Gibou, F., Fedkiw, R., Caflisch, R., and Osher, S. (2003). “A Level Set Approach for the Numerical Simulation of Dendritic Growth”. *Journal of Scientific Computing*, 19 (1-3), pp. 183–199. URL: <http://link.springer.com/article/10.1023/A%3A1025399807998> (cited on page 25).
- [Gouttebroze 2005]**
Gouttebroze, S. (2005). “Modélisation 3d par éléments finis de la macroségrégation lors de la solidification d'alliages binaires”. PhD thesis. École Nationale Supérieure des Mines de Paris. URL: <https://pastel.archives-ouvertes.fr/pastel-00001885/document> (cited on page 12).
- [Guo et al. 2003]**
Guo, J. and Beckermann, C. (2003). “Three-Dimensional Simulation of Freckle Formation During Binary Alloy Solidification: Effect of Mesh Spacing”. *Numerical Heat Transfer, Part A: Applications*, 44 (6). <http://dx.doi.org/10.1080/716100512>, pp. 559–576. URL: <http://user.engineering.uiowa.edu/~becker/documents.dir/GuoFreckle.pdf>.
- [Hachani et al. 2012]**
Hachani, L. et al. (2012). “Experimental analysis of the solidification of Sn–3 wt.%Pb alloy under natural convection”. *International Journal of Heat and Mass Transfer*, 55 (7–8), pp. 1986–1996. URL: <http://www.sciencedirect.com/science/article/pii/S0017931011007009> (cited on page 7).
- [Hachem et al. 2010]**
Hachem, E., Rivaux, B., Kloczko, T., Digonnet, H., and Coupez, T. (2010). “Stabilized finite element method for incompressible flows with high Reynolds number”. *Journal of Computational Physics*, 229 (23), pp. 8643–8665. URL: <http://www.sciencedirect.com/science/article/pii/S0021999110004237>.
- [Hachem 2009]**
Hachem, E. (2009). “Stabilized finite element method for heat transfer and turbulent flows inside industrial furnaces”. PhD Thesis. École Nationale Supérieure des Mines de Paris. URL: <https://tel.archives-ouvertes.fr/tel-00443532>.
- [Harlow et al. 1965]**
Harlow, F. H. and Welch, J. E. (1965). “Numerical Calculation of Time-Dependent Viscous Incompressible Flow of Fluid with Free Surface”. *Physics of Fluids (1958-1988)*, 8 (12), pp. 2182–2189. URL: <http://scitation.aip.org/content/aip/journal/pof1/8/12/10.1063/1.1761178> (cited on page 25).
- [Hebditch et al. 1974]**
Hebditch, D. J. and Hunt, J. D. (1974). “Observations of ingot macrosegregation on model systems”. *Metallurgical Transactions*, 5 (7), pp. 1557–1564. URL: <http://link.springer.com/article/10.1007/BF02646326> (cited on page 7).

Bibliography

[Hirt 1971]

Hirt, C. W. (1971). "An arbitrary Lagrangian-Eulerian computing technique". *Proceedings of the Second International Conference on Numerical Methods in Fluid Dynamics*. Ed. by M. Holt. Lecture Notes in Physics 8. Springer Berlin Heidelberg, pp. 350–355. URL: http://link.springer.com/chapter/10.1007/3-540-05407-3_50 (cited on page 25).

[Hirt et al. 1981]

Hirt, C. W and Nichols, B. D (1981). "Volume of fluid (VOF) method for the dynamics of free boundaries". *Journal of Computational Physics*, 39 (1), pp. 201–225. URL: <http://www.sciencedirect.com/science/article/pii/0021999181901455> (cited on page 25).

[Hysing et al. 2009]

Hysing, S. et al. (2009). "Quantitative benchmark computations of two-dimensional bubble dynamics". *International Journal for Numerical Methods in Fluids*, 60 (11), pp. 1259–1288. URL: <http://onlinelibrary.wiley.com/doi/10.1002/fld.1934/abstract> (cited on page 33).

[Karagadde et al. 2014]

Karagadde, S., Yuan, L., Shevchenko, N., Eckert, S., and Lee, P. D. (2014). "3-D microstructural model of freckle formation validated using in situ experiments". *Acta Materialia*, 79, pp. 168–180. URL: <http://www.sciencedirect.com/science/article/pii/S1359645414004984>.

[Karma et al. 1996]

Karma, A. and Rappel, W.-J. (1996). "Phase-field method for computationally efficient modeling of solidification with arbitrary interface kinetics". *Physical Review E*, 53 (4), R3017–R3020. URL: <http://link.aps.org/doi/10.1103/PhysRevE.53.R3017> (cited on page 25).

[Khan et al. 2014]

Khan, M. I., Mostafa, A. O., Aljarrah, M., Essadiqi, E., and Medraj, M. (2014). "Influence of Cooling Rate on Microsegregation Behavior of Magnesium Alloys". *Journal of Materials*, 2014, e657647. URL: <http://www.hindawi.com/journals/jma/2014/657647/abs/> (cited on page 17).

[Kobayashi 1988]

Kobayashi, S. (1988). "Solute redistribution during solidification with diffusion in solid phase: A theoretical analysis". *Journal of Crystal Growth*, 88 (1), pp. 87–96. URL: <http://www.sciencedirect.com/science/article/pii/S0022024898900100> (cited on page 17).

[Kohler 2008]

Kohler, F. (2008). "Peritectic solidification of Cu-Sn alloys: microstructure competition at low speed". PhD Thesis. EPFL.

[Lesoult 2005]

Lesoult, G. (2005). "Macrosegregation in steel strands and ingots: Characterisation, formation and consequences". *Materials Science and Engineering: A*, International Con-

- ference on Advances in Solidification Processes 413–414, pp. 19–29. URL: <http://www.sciencedirect.com/science/article/pii/S0921509305010063> (cited on pages 3, 7).
- [Lesoult et al. 2001]**
Lesoult, G. et al. (2001). “Equi-axed growth and related segregations in cast metallic alloys”. *Science and Technology of Advanced Materials*, 2 (1), p. 285. URL: <http://iopscience.iop.org/1468-6996/2/1/A55> (cited on page 7).
- [Liu 2005]**
Liu, W. (2005). “Finite Element Modelling of Macrosegregation and Thermomechanical Phenomena in Solidification Processes”. PhD thesis. École Nationale Supérieure des Mines de Paris. URL: <http://pastel.archives-ouvertes.fr/pastel-00001339> (cited on page 12).
- [Maitre 2006]**
Maitre, E. (2006). “Review of numerical methods for free interfaces”. Les Houches, France. URL: <http://goo.gl/Re6f3a> (cited on page 25).
- [Martorano et al. 2003]**
Martorano, M. A., Beckermann, C., and Gandin, C.-A. (2003). “A solutal interaction mechanism for the columnar-to-equiaxed transition in alloy solidification”. *Metallurgical and Materials Transactions A*, 34 (8), pp. 1657–1674. URL: <http://link.springer.com/article/10.1007/s11661-003-0311-x> (cited on page 17).
- [Mesri et al. 2009]**
Mesri, Y., Digonnet, H., and Coupez, T. (2009). “Advanced parallel computing in material forming with CIMLib”. *European Journal of Computational Mechanics/Revue Européenne de Mécanique Numérique*, 18 (7-8), pp. 669–694. URL: <http://www.tandfonline.com/doi/abs/10.3166/ejcm.18.669-694> (cited on page 13).
- [Mosbah 2008]**
Mosbah, S. (2008). “Multiple scales modeling of solidification grain structures and segregation in metallic alloys”. PhD thesis. École Nationale Supérieure des Mines de Paris. URL: <https://tel.archives-ouvertes.fr/tel-00349885/document> (cited on page 12).
- [Ni et al. 1991]**
Ni, J. and Beckermann, C. (1991). “A volume-averaged two-phase model for transport phenomena during solidification”. *Metallurgical Transactions B*, 22 (3), pp. 349–361. URL: <http://link.springer.com/article/10.1007/BF02651234> (cited on pages 17, 18, 20).
- [Osher et al. 1988]**
Osher, S. and Sethian, J. A. (1988). “Fronts propagating with curvature-dependent speed: Algorithms based on Hamilton-Jacobi formulations”. *Journal of Computational Physics*, 79 (1), pp. 12–49. URL: <http://www.sciencedirect.com/science/article/pii/0021999188900022> (cited on pages 25, 26).

Bibliography

[Osher et al. 2003]

Osher, S. and Fedkiw, R. (2003). "Signed Distance Functions". *Level Set Methods and Dynamic Implicit Surfaces*. Applied Mathematical Sciences 153. Springer New York, pp. 17–22. URL: http://link.springer.com/chapter/10.1007/0-387-22746-6_2 (cited on page 35).

[Peng et al. 1999]

Peng, D., Merriman, B., Osher, S., Zhao, H., and Kang, M. (1999). "A PDE-Based Fast Local Level Set Method". *Journal of Computational Physics*, 155 (2), pp. 410–438. URL: <http://www.sciencedirect.com/science/article/pii/S0021999199963453> (cited on pages 28, 34).

[Pickering 2013]

Pickering, E. J. (2013). "Macrosegregation in Steel Ingots: The Applicability of Modelling and Characterisation Techniques". *ISIJ International*, 53 (6), pp. 935–949.

[Poirier 1987]

Poirier, D. R. (1987). "Permeability for flow of interdendritic liquid in columnar-dendritic alloys". *Metallurgical Transactions B*, 18 (1), pp. 245–255. URL: <http://link.springer.com/article/10.1007/BF02658450> (cited on page 6).

[Pollock et al. 1996]

Pollock, T. M. and Murphy, W. H. (1996). "The breakdown of single-crystal solidification in high refractory nickel-base alloys". *Metallurgical and Materials Transactions A*, 27 (4), pp. 1081–1094. URL: <http://link.springer.com/article/10.1007/BF02649777>.

[Prescott et al. 1994]

Prescott, P. J., Incropera, F. P., and Gaskell, D. R. (1994). "Convective Transport Phenomena and Macrosegregation During Solidification of a Binary Metal Alloy: II—Experiments and Comparisons With Numerical Predictions". *Journal of Heat Transfer*, 116 (3), pp. 742–749. URL: <http://dx.doi.org/10.1115/1.2910930> (cited on page 7).

[Prosperetti 2002]

Prosperetti, A. (2002). "Navier-Stokes Numerical Algorithms for Free-Surface Flow Computations: An Overview". *Drop-Surface Interactions*. Ed. by M. Rein. CISM International Centre for Mechanical Sciences 456. Springer Vienna, pp. 237–257. URL: http://link.springer.com/chapter/10.1007/978-3-7091-2594-6_8 (cited on page 25).

[Ramirez et al. 2003]

Ramirez, J. C. and Beckermann, C. (2003). "Evaluation of a rayleigh-number-based freckle criterion for Pb-Sn alloys and Ni-base superalloys". *Metallurgical and Materials Transactions A*, 34 (7), pp. 1525–1536. URL: <http://link.springer.com/article/10.1007/s11661-003-0264-0> (cited on page 6).

[Rappaz et al. 2003]

Rappaz, M., Bellet, M., and Deville, M. (2003). *Numerical Modeling in Materials Science and Engineering*. Springer Series in Computational Mathematics. Springer Berlin Heidelberg (cited on pages 6, 19, 92).

[Rivaux 2011]

Rivaux, B. (2011). "Simulation 3D éléments finis des macroségrégations en peau induites par déformations thermomécaniques lors de la solidification d'alliages métalliques". PhD Thesis. École Nationale Supérieure des Mines de Paris. URL: <http://pastel.archives-ouvertes.fr/pastel-00637168> (cited on page 12).

[Sarazin et al. 1992]

Sarazin, J. R. and Hellawell, A. (1992). "Studies of Channel-Plume Convection during Solidification". *Interactive Dynamics of Convection and Solidification*. Ed. by S. H. Davis, H. E. Huppert, U. Müller, and M. G. Worster. NATO ASI Series 219. Springer Netherlands, pp. 143–145. URL: http://link.springer.com/chapter/10.1007/978-94-011-2809-4_22 (cited on page 10).

[Schneider et al. 1997]

Schneider, M. C., Gu, J. P., Beckermann, C., Boettinger, W. J., and Kattner, U. R. (1997). "Modeling of micro- and macrosegregation and freckle formation in single-crystal nickel-base superalloy directional solidification". *Metallurgical and Materials Transactions A*, 28 (7), pp. 1517–1531. URL: <http://link.springer.com/article/10.1007/s11661-997-0214-3> (cited on page 10).

[Sethian 1996]

Sethian, J. A. (1996). "A fast marching level set method for monotonically advancing fronts". *Proceedings of the National Academy of Sciences*, 93 (4), pp. 1591–1595. URL: <http://www.pnas.org/content/93/4/1591> (cited on page 35).

[Shakoor et al. 2015]

Shakoor, M., Scholtes, B., Bouchard, P.-O., and Bernacki, M. (2015). "An efficient and parallel level set reinitialization method - Application to micromechanics and microstructural evolutions". *Applied Mathematical Modelling (submitted)*, (cited on page 35).

[Shevchenko et al. 2013]

Shevchenko, N., Boden, S., Gerbeth, G., and Eckert, S. (2013). "Chimney Formation in Solidifying Ga-25wt pct In Alloys Under the Influence of Thermosolutal Melt Convection". *Metallurgical and Materials Transactions A*, 44 (8), pp. 3797–3808. URL: <http://link.springer.com/article/10.1007/s11661-013-1711-1> (cited on page 10).

[Strotos et al. 2008]

Strotos, G., Gavaises, M., Theodorakakos, A., and Bergeles, G. (2008). "Numerical investigation of the cooling effectiveness of a droplet impinging on a heated surface". *International Journal of Heat and Mass Transfer*, 51 (19–20), pp. 4728–4742. URL: <http://www.sciencedirect.com/science/article/pii/S001793100800149X> (cited on page 30).

[Süli 2000]

Süli, E. (2000). *Lecture Notes on Finite Element Methods for Partial Differential Equations*.

[Sun et al. 2004]

Sun, Y. and Beckermann, C. (2004). "Diffuse interface modeling of two-phase flows

Bibliography

based on averaging; mass and momentum equations". *Physica D: Nonlinear Phenomena*, 198 (3–4), pp. 281–308. URL: <http://www.sciencedirect.com/science/article/pii/S0167278904003689> (cited on page 27).

[Sussman et al. 1994]

Sussman, M., Smereka, P., and Osher, S. (1994). "A Level Set Approach for Computing Solutions to Incompressible Two-Phase Flow". *Journal of Computational Physics*, 114 (1), pp. 146–159. URL: <http://www.sciencedirect.com/science/article/pii/S0021999184711557> (cited on pages 33, 34).

[Swaminathan. et al. 1993]

Swaminathan., C. R. and Voller, V. R. (1993). "On The Enthalpy Method". *International Journal of Numerical Methods for Heat & Fluid Flow*, 3 (3), pp. 233–244. URL: <http://www.emeraldinsight.com/journals.htm?articleid=1665561&show=abstract>.

[Tan et al. 2007]

Tan, L. and Zabaras, N. (2007). "A level set simulation of dendritic solidification of multi-component alloys". *Journal of Computational Physics*, 221 (1), pp. 9–40. URL: <http://www.sciencedirect.com/science/article/pii/S0021999106002737> (cited on page 25).

[TCBIN 2006]

TCBIN (2006). *TCBIN: TC Binary Solutions Database*. Stockholm, SE.

[TCFE6 2010]

TCFE6 (2010). *TCFE6: a thermodynamic database for different kinds of steels and Fe-based alloys*. Stockholm, SE. URL: <http://goo.gl/qiD3kE>.

[Thuin et al. 2004]

Thuinet, L. and Combeau, H. (2004). "Prediction of macrosegregation during the solidification involving a peritectic transformation for multicomponent steels". *Journal of Materials Science*, 39 (24), pp. 7213–7219. URL: <http://link.springer.com/article/10.1023/B%3AJMSC.0000048734.34597.1e>.

[Tiller et al. 1953]

Tiller, W. A, Jackson, K. A, Rutter, J. W, and Chalmers, B (1953). "The redistribution of solute atoms during the solidification of metals". *Acta Metallurgica*, 1 (4), pp. 428–437. URL: <http://www.sciencedirect.com/science/article/pii/0001616053901266> (cited on page 5).

[Tourret et al. 2009]

Tourret, D. and Gandin, C. A. (2009). "A generalized segregation model for concurrent dendritic, peritectic and eutectic solidification". *Acta Materialia*, 57 (7), pp. 2066–2079. URL: <http://www.sciencedirect.com/science/article/pii/S1359645409000184> (cited on page 17).

[Vigneaux 2007]

Vigneaux, P. (2007). "Méthodes Level Set pour des problèmes d'interface en microflu-

idique". PhD thesis. Université Sciences et Technologies - Bordeaux I. URL: <https://tel.archives-ouvertes.fr/tel-00189409/document> (cited on page 34).

[Ville et al. 2011]

Ville, L., Silva, L., and Coupez, T. (2011). "Convected level set method for the numerical simulation of fluid buckling". *International Journal for Numerical Methods in Fluids*, 66 (3), pp. 324–344. URL: <http://onlinelibrary.wiley.com/doi/10.1002/fld.2259/abstract> (cited on page 34).

[Voller et al. 1989]

Voller, V. R., Brent, A. D., and Prakash, C. (1989). "The modelling of heat, mass and solute transport in solidification systems". *International Journal of Heat and Mass Transfer*, 32 (9), pp. 1719–1731. URL: <http://www.sciencedirect.com/science/article/pii/0017931089900549> (cited on page 98).

[Wang et al. 1993]

Wang, C. Y. and Beckermann, C. (1993). "A multiphase solute diffusion model for dendritic alloy solidification". *Metallurgical Transactions A*, 24 (12), pp. 2787–2802. URL: <http://link.springer.com/article/10.1007/BF02659502> (cited on page 17).

[Wanqi et al. 1989]

Wanqi, J. I. E. and Yaohe, Z. (1989). "Formation of hot-top segregation in steel ingot and effect of steel compositions". *Metallurgical Transactions B*, 20 (5), pp. 723–730. URL: <http://link.springer.com/article/10.1007/BF02655930> (cited on page 7).

[WSA 2014]

WSA (2014). *World Steel Association: Statistics archive*. URL: <http://www.worldsteel.org/statistics/statistics-archive.html> (cited on page 10).

[Xu et al. 1991]

Xu, D. and Li, Q. (1991). "Gravity- and Solidification-Shrinkage-Induced Liquid Flow in a Horizontally Solidified Alloy Ingot". *Numerical Heat Transfer, Part A: Applications*, 20 (2), pp. 203–221. URL: <http://dx.doi.org/10.1080/10407789108944817> (cited on page 6).

[Yuan et al. 2012]

Yuan, L. and Lee, P. D. (2012). "A new mechanism for freckle initiation based on microstructural level simulation". *Acta Materialia*, 60 (12), pp. 4917–4926. URL: <http://www.sciencedirect.com/science/article/pii/S1359645412003205>.